Environmental Science & Technology

pubs.acs.org/est

Article

Global Health and Climate Effects of Organic Aerosols from Different Sources

Duseong S. Jo,* Benjamin A. Nault, Simone Tilmes, Andrew Gettelman, Christina S. McCluskey, Alma Hodzic, Daven K. Henze, Muhammad Omar Nawaz, Ka Ming Fung, and Jose L. Jimenez

Cite This: *Environ. Sci. Technol.* 2023, 57, 13793−13807

Read Online

ACCESS | Metrics & More | Article Recommendations | Supporting Information

ABSTRACT: The impact of aerosols on human health and climate is well-recognized, yet many studies have only focused on total $PM_{2.5}$ or changes from anthropogenic activities. This study quantifies the health and climate effects of organic aerosols (OA) from anthropogenic, biomass burning, and biogenic sources. Using two atmospheric chemistry models, CAM-chem and GEOS-Chem, our findings reveal that anthropogenic primary OA (POA) has the highest efficiency for health effects but the lowest for direct radiative effects due to spatial and temporal variations associated with population and surface albedo. The treatment of POA as nonvolatile or semivolatile also influences these efficiencies through different chemical processes. Biogenic OA shows moderate efficiency for health effects and the highest for direct radiative effects but has the lowest efficiency for indirect effects due to the reduced high cloud, caused by stabilized temperature profiles from aerosol−radiation interactions in biogenic OA-rich regions. Biomass burning OA is important for cloud radiative effect changes in remote atmospheres due to its ability to be transported further than other OAs. This study highlights the importance of not only OA characteristics such as toxicity and refractive index but also atmospheric processes such as transport and chemistry in determining health and climate impact efficiencies.

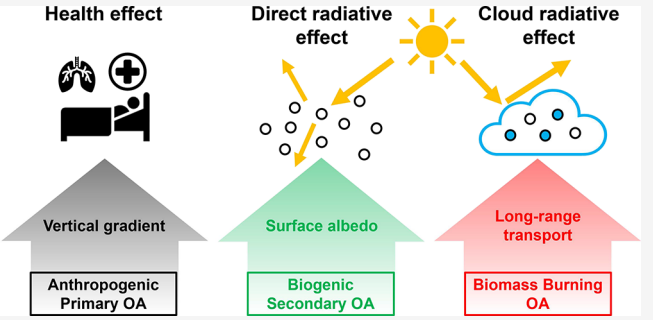

KEYWORDS: *organic aerosols, atmospheric chemistry modeling, health impact, aerosol−radiation interactions, aerosol−cloud interactions*

1. INTRODUCTION

Atmospheric aerosols play a major role in the Earth system, impacting climate, health, visibility, and atmospheric chemistry.[1−4] Major aerosol types in chemistry models include sulfate, nitrate, ammonium, organic aerosol (OA), black carbon (BC), dust, and sea salt.[5] These various constituents of aerosols introduce substantial uncertainties when estimating the impacts of aerosols on human health and climate effects.[4,6] In particular, OA makes up a substantial portion of the submicrometer aerosol mass,[7] but its simulation in atmospheric chemistry models has been extremely challenging over the past two decades.[8−10] This can be attributed to the complexity of the chemical processes of OA with 10,000 to 100,000 different organic compounds existing in the atmosphere,[11] particularly for secondary OA (SOA), which is formed in the atmosphere through the oxidation of volatile organic compounds (VOCs).

While it is clear that reducing aerosols is beneficial for human health, it can result in disbenefits for near-term climate change. The extent of these trade-offs when addressing climate change mitigation policies has not been fully addressed.[12,13] Furthermore, aerosols are not as evenly distributed as long-lived greenhouse gases, which leads to their health and climate effects being influenced by the location of their sources, chemical transformation, and loss processes.

Unlike other aerosols, atmospheric OA comes from diverse sources, including anthropogenic, biomass burning, biogenic, and marine emissions, as well as different formation processes such as primary OA (POA) and SOA.[14] These varying characteristics of OA can result in different spatial and temporal distributions, leading to different implications in the Earth system.

Given the large mass fraction of OA in submicrometer aerosols (20−90%),[7,15] the role of OA in health and climate effects is considerable. For example, Nault et al.[16] calculated that the reduction in mortality due to $PM_{2.5}$ upon the removal of anthropogenic SOA ranged from 6 (Africa) to 43% (North America), depending on the region. Chowdhury et al.[17] estimated that BC, POA, and anthropogenic SOA contributed to 14.4% of excess deaths from exposure to $PM_{2.5}$, and this

Received: April 14, 2023
Revised: August 21, 2023
Accepted: August 22, 2023
Published: September 6, 2023

estimate increased to 36.4−38.0% when assuming enhanced toxicity of carbonaceous aerosols.

For climate effects, Heald et al.[18] showed that the global direct radiative effect (DRE) by OA (−0.42 W m^{-2}) is comparable to the DRE by sulfate (−0.35 W m^{-2}) or even the sum of sulfate-nitrate-ammonium (SNA) (−0.512 W m^{-2}). Spracklen et al.[19] estimated a DRE of −0.26 W m^{-2} and a first aerosol indirect effect of −0.6 W m^{-2} by anthropogenically controlled SOA. Sporre et al.[20] showed that the removal of isoprene (a major precursor for biogenic SOA) resulted in substantial changes in the cloud radiative effect, ranging from −0.82 to 0.53 W m^{-2} across three different Earth system models. Measurement studies have also identified OA as a key component of cloud condensation nuclei (CCN),[21] in urban,[22] urban downwind,[23] and forest[24] environments.

Recent model evaluation studies in the 2020s have shown that atmospheric chemistry models have significantly improved in terms of reproducing OA against global aircraft observations, at least for a few global models.[25,26] This improvement can be attributed to advancements in OA simulation schemes over the past two decades,[21] such as explicit simulation of isoprene SOA,[27] updated parameters in the volatility basis set (VBS) approach,[28,29] and empirical SOA schemes based on field measurements.[16,30] However, there are still shortcomings in the models. For example, Hodzic et al.[26] reported that POA is overestimated while SOA is underestimated compared to aircraft observations.

In this study, we examine the health and climate (direct and indirect) effects of various OA sources. We utilize two independent global atmospheric chemistry models, CAM-chem and GEOS-Chem, which have different SOA schemes, chemical mechanisms, and horizontal and vertical resolutions. The two models used in this study show reduced model variability and also better agreement with OA observations from the ATom campaign compared to the models in the AeroCom intercomparison.[26] This approach allows us to address the variabilities present in model simulations while ensuring that we stay within an observationally constrained boundary. In order to further reduce the model uncertainties, we calculate health and climate effects in terms of not only the absolute magnitude but also efficiencies (impacts per atmospheric burden). This allows us to normalize potentially overestimated or underestimated specific OA mass concentrations on health and climate effects. We also compare the effects of nonvolatile and semivolatile POA simulations in GEOS-Chem. To address uncertainties related to health and climate effect calculations, we estimate health effects using two different methods and calculate DRE under both clear- and all-sky conditions. For the calculations of aerosol−cloud interaction, we reduce the nonlinearity by running the model with a specified dynamics setup, combining POA and SOA to increase the signal-to-noise ratio, and executing multiyear simulations that take into account daily and diurnal variations.

Detailed descriptions of the modeling framework, OA simulations, health effect calculations, and climate effect estimates for aerosol−radiation and aerosol−cloud interactions can be found in Section 2. The health and climate effect results for each OA category are presented in Section 3. Section 4 contains discussions and implications from this work.

2. MODELS AND ANALYSIS

2.1. Model Descriptions and OA Simulations. Here, we provide descriptions of the two global atmospheric chemistry models (GEOS-Chem and CAM-chem) used in this study. The simulation performance of OA in both models has been evaluated against field observations in numerous previous studies.[25−28,30−38] Both models have also participated in various global model intercomparison studies focusing on aerosols.[10,39−49]

First, we use the GEOS-Chem[50] 12.6.1 with additional updates to separate OA into anthropogenic POA (ANPOA), biomass burning POA (BBPOA), marine POA (MPOA), anthropogenic SOA (ANSOA), biomass burning SOA (BBSOA), and biogenic SOA (BGSOA). Two tracers are used for each POA type: hydrophobic (OCPO) and hydrophilic (OCPI) with an e-folding time of 1.15 days for the conversion of hydrophobic to hydrophilic tracer.[51] MPOA is also calculated based on these two tracers, one for hydrophobic and the other for hydrophilic.[52] ANSOA and BBSOA are simulated using the SIMPLE parameterization based on field OA measurements,[53] but ANSOA is further updated to reflect recent findings on the relationship between ANSOA enhancement and aromatics reactivities.[16] It is worth noting that the VBS scheme in GEOS-Chem underestimated the urban SOA during the urban field campaign, whereas the SIMPLE SOA scheme did not.[31] McDuffie et al.[54] also used the SIMPLE SOA scheme for their health effect calculation using GEOS-Chem. SOA from monoterpenes and sesquiterpenes is simulated using the volatility basis set (VBS) approach, as implemented by Pye et al.[55] Isoprene SOA is explicitly simulated using the aqueous phase mechanism by Marais et al.[27] POAs are assumed as nonvolatile in the standard simulation, but, additionally, a semivolatile POA (SVPOA) option is performed to examine the differences in results between nonvolatile and semivolatile assumptions for ANPOA and BBPOA. SVPOA from semivolatile organic compounds (SVOCs) is calculated using the two-product approach with aging reactions that decrease saturation vapor pressure by 100 times. SVPOA from intermediate-volatile organic compounds (IVOCs) is simulated using the VBS approach.[37]

Second, the Community Atmosphere Model with chemistry version 6 (CAM6-chem), a detailed chemistry version of the Community Earth System Model (CESM)[56] version 2.2, is used with the same separations of OA in GEOS-Chem, but MPOA is not available in the model.[57]

Unlike GEOS-Chem, which uses a bulk aerosol scheme, CAM-chem uses a four-mode version of the Modal Aerosol Module (MAM4).[58] ANPOA and BBPOA are emitted as the primary carbon mode and converted to the accumulation mode through microphysical aging processes such as coagulation.[59] Aitken and accumulation modes are used to calculate the microphysics of SOA. The organic nucleation process is not included in the model at present. The model only accounts for sulfuric acid vapor homogeneous nucleation through a binary parameterization.[59−61] The VBS scheme by Hodzic et al.[28] is used for all SOA, as implemented by Tilmes et al.[34] and further updated for NO_x-dependent pathways by Jo et al.[62] SOA from S/IVOCs is also calculated on the VBS space, by assuming 60% of POA and 20% of nonmethane VOC (NMVOCs) as SVOC and IVOC emissions, respectively. In addition to OA, both models simulate secondary inorganic aerosols, black carbon, dust, and sea salt aerosols. However, CAM-chem[57] only simulates sulfate (considered to be ammonium bisulfate), while GEOS-Chem[63] calculates sulfate, nitrate, and ammonium using the ISORROPIA II thermody-

https://doi.org/10.1021/acs.est.3c02823
Environ. Sci. Technol. 2023, 57, 13793−13807

namic model[64] for secondary inorganic aerosols. Moreover, CAM-chem allows for aerosols to affect meteorological fields, including cloud properties, through two-way interactions, whereas meteorological fields are fixed in GEOS-Chem.

We run both models for the year 2010, with an additional three-month spin-up period. Furthermore, to account for potential influences of year-to-year changes in the cloud cover and location on aerosol−cloud interaction calculations (Section 2.4), we extend the CAM-chem simulation for an additional four years.

GEOS-Chem is a chemical transport model (CTM) driven by assimilated meteorological fields; here, we use the Modern-Era Retrospective Analysis for Research and Applications version 2 (MERRA2).[65] CAM-chem has its own dynamic core, but temperature and winds are nudged to the MERRA2 meteorology in this study to reduce the uncertainty associated with dynamics.

Nudging occurs at each time step using the next target nudging force option and the weak timescale option.[38] Horizontal resolutions of 2° × 2.5° and 0.95° × 1.25° are used for GEOS-Chem and CAM-chem, respectively, with 47 and 32 vertical levels. We use the Community Emissions Data System (CEDS) inventory[66] for anthropogenic emissions and the Global Fire Emission Database (GFED) version 4[67] for biomass burning emissions in both models. However, for anthropogenic SOA precursor emissions in GEOS-Chem, we use the Hemispheric Transport of Air Pollution version 2 (HTAPv2) inventory.[68] The HTAP best reproduced the observed relationship between CO and aromatics from 11 major urban field studies, which is a critical factor for the SIMPLE SOA scheme developed by Nault et al.[16] For example, the HTAP showed an R^2 of 0.54 while the CEDS showed an R^2 of 0.26 when compared to field campaign observations.[16] Our calculation shows that switching from HTAP to CEDS for anthropogenic SOA emission increases the emission by 23%. Biogenic emissions are calculated online using the Model of Emissions of Gases and Aerosols from Nature version 2.1 (MEGANv2.1) algorithm in both models.[69] MPOA in GEOS-Chem is also calculated online based on Gantt et al.[52]

2.2. Health Impact Estimates. We estimate the premature deaths associated with exposure to OA by combining population data from the Columbia University Center for International Earth Science Information Network (CIESIN)[70] with baseline mortality rates from the Global Burden of Disease (GBD) study (2015)[71] for the following diseases: ischemic heart disease, stroke, chronic obstructive pulmonary disease, lung cancer, and acute lower respiratory illness. To address uncertainties related to premature death calculation methods, we calculate the relative risk from $PM_{2.5}$ (particulate matter with a particle diameter smaller than 2.5 μm) exposure using two methods: the integrated exposure-response (IER)[72] and the global exposure mortality model (GEMM).[73] The calculations are based on annual average surface-level $PM_{2.5}$ concentrations, populations, and disease-specific parameters such as $PM_{2.5}$ threshold values.

The premature deaths attributed to each OA category are calculated using the method outlined by Nault et al.[16] This involves subtracting the OA concentration from the total $PM_{2.5}$ concentration to calculate the difference in deaths caused by the total $PM_{2.5}$ and the reduced $PM_{2.5}$. To reduce uncertainties due to the coarse spatial resolutions of models, satellite-derived $PM_{2.5}$ concentrations at a 0.1° × 0.1° resolution (V5.GL.03) based on van Donkelaar et al.[74] are used to determine the total $PM_{2.5}$ concentration. These satellite-derived $PM_{2.5}$ concentrations correspond to the same years as our GEOS-Chem and CESM simulations, minimizing potential discrepancies arising from interannual variability in OA sources. We also calculated health impacts using another satellite product (V4.GL.02)[75] and found no significant differences between the two satellite products in terms of health effect estimates.

OA concentrations are recalculated for health impact assessment using the fraction of each simulated OA component to the total modeled $PM_{2.5}$, multiplied by the higher-resolution satellite-based $PM_{2.5}$ concentrations. The impact of secondary inorganic aerosol is also calculated for comparison to the effect of OA. Further information on the downscaling and rescaling methods, health impact calculations, and related parameters can be found in Nault et al.[16] and Nawaz et al.[76]

2.3. Aerosol−Radiation Interaction (Direct Effect). Online radiative transfer calculations are available for both CAM-chem and GEOS-Chem using the rapid radiative transfer method for general circulation models (RRTMG).[77] We calculate the direct radiative effect (DRE) of OA under both clear- and all-sky conditions. Only shortwave flux changes are considered in this study as the longwave DREs of OA are negligible globally.[18] Shortwave fluxes are calculated over 14 wavelength bands from 0.2 to 12.2 μm. The aerosol optical depth (AOD), single scattering albedo, and asymmetry parameters are calculated using a look-up table approach with precalculated aerosol optical properties using Mie theory, as a function of wavelength and relative humidity (RH). We do not consider brown carbon in this calculation, which is a limitation of this study. The contribution of brown carbon absorption to the negative DRE of OA varies greatly across studies, and we have addressed this in detail in Section 4.

The hygroscopic growth factors applied to each model are different. CAM-chem uses the Optical Properties of Aerosols and Clouds (OPAC).[78] The factors used in GEOS-Chem are originally based on OPAC but updated with findings from other previous studies.[79,80] Both models divide OA into hydrophobic and hydrophilic components, and hygroscopic growths are considered only for hydrophilic components. However, the classification method is different for each model. CAM-chem assumes all POAs (in both primary carbon and accumulation modes) as hydrophobic, while GEOS-Chem assumes only hydrophobic POA (OCPO; nonvolatile simulation) or fresh POA (semivolatile simulation) as hydrophobic, with the rest being hydrophilic POA. Furthermore, GEOS-Chem assumes external mixing, while CAM-chem assumes external mixing between modes but internal mixing within each mode.

For size distributions of OA, a single geometric mean dry radius of 0.058 μm and a standard deviation of 1.6 are assumed in the bulk aerosol scheme in GEOS-Chem.[81] On the other hand, in CAM-chem, the radius of each mode is calculated online from the number concentration, and a standard deviation of 1.6 is also used for Aitken, accumulation, and primary carbon modes.[59,82] The typical size ranges are 0.06−0.30 μm for the primary carbon mode, 0.015−0.053 μm for the Aitken mode, and 0.058−0.48 μm for the accumulation mode, respectively.[61] In the CAM-chem simulations in this study, the accumulation mode comprises 93% of OA followed by 6% for the primary carbon mode and 1% for the Aitken mode, which

https://doi.org/10.1021/acs.est.3c02823
Environ. Sci. Technol. 2023, 57, 13793−13807

is consistent with Tilmes et al.[34] The column version of RRTMG is also used for the offline analysis in Section 3.

2.4. Aerosol−Cloud Interaction (Indirect Effect). Since GEOS-Chem is a CTM, meaning that there is no two-way interaction between aerosol and meteorology, we estimate the aerosol indirect effects using only the CAM-chem model. Aerosol interactions with cloud microphysics are represented in CAM-chem with the MG2 scheme.[83] To assess the impact of each individual OA component, sensitivity simulations are performed by removing each OA component (including the "all OA" case) in the model while keeping other aerosols fixed. The changes in shortwave and longwave cloud radiative effects between the base and sensitivity simulations are then calculated. In this way, we consider not only the first indirect effect (increasing cloud condensation nuclei and cloud droplet numbers)[84] and the second indirect effect (reduced precipitation due to smaller droplets and increased cloud cover/lifetime)[85] but also cloud adjustments in response to the changes in the atmosphere and land surface.

Unlike health impacts and DRE calculations in which aerosol loadings and effects are generally proportional to each other (although still nonlinear), cloud response to aerosols is highly nonlinear (even the sign can be changed) due to a number of different cloud types and regimes and the micro- and macrophysical influences on the cloud formation.[86] Therefore, additional steps are taken in the simulations to reduce the uncertainties related to the cloud radiative effect change calculations. (1) We run the model in a specified dynamics setup (temperature and winds are nudged to MERRA2) to minimize nonlinearity and model internal variability. (2) POA and SOA are lumped together for each source to obtain a higher signal-to-noise ratio in this analysis. (3) Unlike health effects and DRE calculations, the indirect effect of secondary inorganic aerosol is not calculated to prevent inaccuracies in the cloud microphysics that would result from the elimination of sulfate. (4) We save the model output every 25 h to consider diurnal variations of cloud properties (e.g., shifting the local time of saved output by 1 h with each subsequent day) and present the variability range based on the ±1 standard deviation. (5) Calculations are based on results from a five-year period (2010−2014), instead of a single-year simulation.

3. RESULTS

3.1. Health Impacts. Figure 1 shows the premature death and DRE caused by OA from various sources, calculated both in terms of the absolute magnitude and efficiency. Secondary inorganic aerosols are also included as a reference for comparison with OA. Secondary inorganic aerosols in both models have been extensively evaluated against surface and aircraft observations.[2,63,87−96] In this study, premature deaths due to $PM_{2.5}$ are calculated to be 3.66 million using the IER method and 8.41 million using the GEMM method. These values align with previous studies which estimated 3.22−4.00 million for the IER method[16,73,97,98] and 7.78−8.92 million for the GEMM method.[16,73,99]

Despite the differences between the two models, two POA treatments, and two mortality calculation methods (Figures S1 and S2), the results clearly show that anthropogenic OA is highly influential for human health, as they are high in areas with large populations (Figure 2 and Figures S3−S9). Given that the 95% confidence intervals for both the IER and GEMM methods fall within a 15−20% range,[73] the higher efficiency of

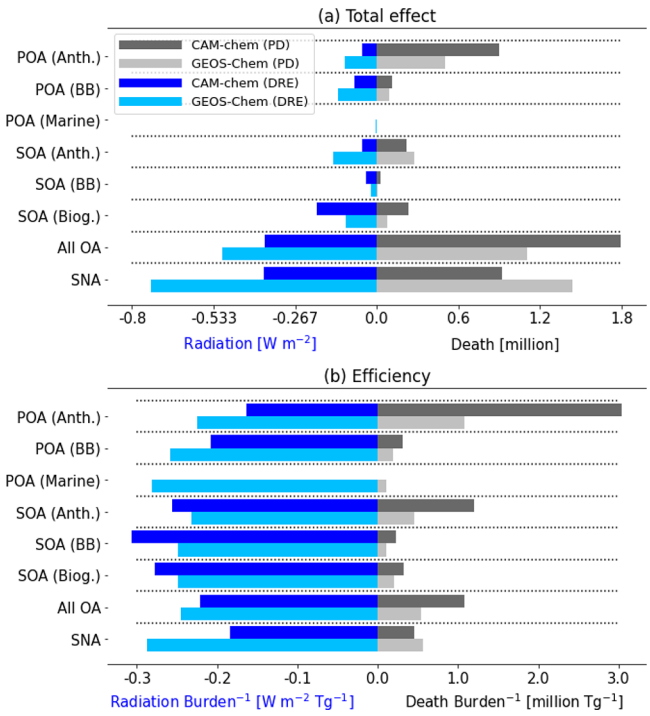

Figure 1. Premature deaths and DREs calculated by CAM-chem (dark gray and blue) and GEOS-Chem (light gray and sky blue) for 2010. (a) Total effect and (b) effect efficiency (impacts per Tg burden). Premature death calculation is based on the IER, and the DRE is for all sky values. SNA is sulfate for CAM-chem and sulfate-nitrate-ammonium for GEOS-Chem. Marine POA is not included in CAM-chem. Premature death calculation based on the GEMM method and clear-sky DRE is shown in Figure S1. The values calculated for each OA category are not additive due to the nonlinear response in health and DRE effects.

anthropogenic OA, POA, and CAM-chem OA is evident. Although the absolute values derived from the IER and GEMM methods are different, the relative differences in health effects attributed to each OA type remain consistent, indicating uniform relative importance across different calculation methods (Figure 2 and Figure S1).

Specifically, aerosol concentrations in areas with populations greater than 1000 per grid point are significant in terms of the absolute magnitude (Figure S3). The relationship between aerosol concentrations and populations (black and magenta lines in Figure S3) also explains the higher health effect efficiencies of OA compared to sulfate in CAM-chem and the similar efficiencies between OA and SNA in GEOS-Chem. In addition to population, there can be other factors such as population age and base mortality rates, which vary among countries. However, these factors do not show a significant relationship with aerosol concentrations in this study. These results are based on the simulation data for 2010; however, our findings suggest that interannual variability is not a major factor in this study. The coefficient of variation (standard deviation over the mean) of interannual variability is at most ∼10% for health effects due to biomass burning OA, which further reduces to ∼5% when calculating effect efficiency (effects per burden). Coefficients of variation for other OAs are calculated to be less than 3%.

Emissions have the most important impact on the distribution of aerosols at the surface and, additionally, on health impacts associated with aerosol exposure due to their

https://doi.org/10.1021/acs.est.3c02823
Environ. Sci. Technol. 2023, 57, 13793−13807

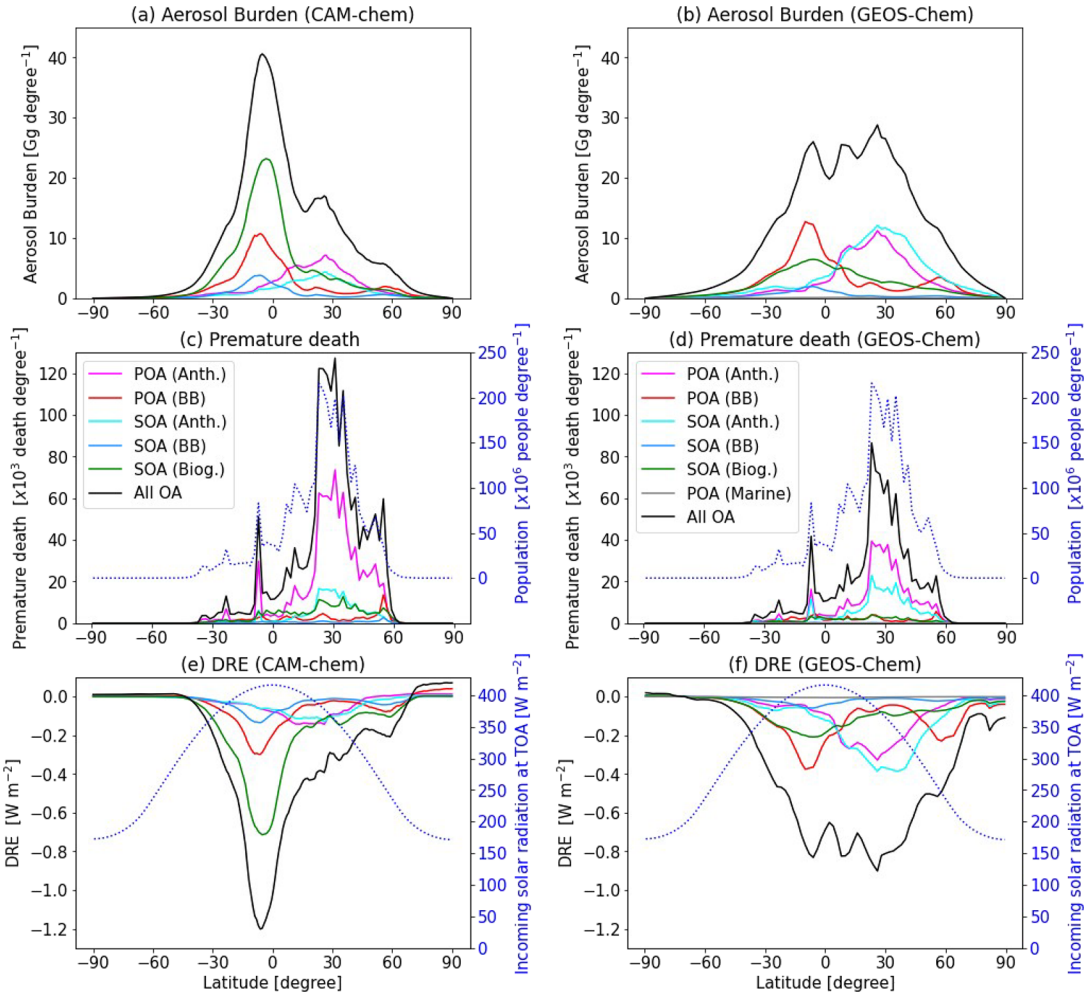

Figure 2. Latitudinal profiles of (a,b) aerosol burden, (c,d) premature death overlaid with population, and (e,f) DRE overlaid with incoming solar radiation at the top of the atmosphere. The left and right columns show the CAM-chem and GEOS-Chem results, respectively. Population data are for 2010 and from the CIESIN.[70] Incoming solar radiation is from Clouds and the Earth's Radiant Energy System.[102]

colocation with areas of the dense population; however, the vertical distribution of aerosols also contributes. Anthropogenic OAs are highly concentrated near the ground where people live, while biogenic and biomass burning OAs have relatively high concentrations up to 600−700 hPa levels (Figures S10−S12). Biomass burning and biogenic OAs are more likely to be transported to the free troposphere via fire-induced convection[100] or upward transport of precursor gases.[101] The vertical distribution also explains the difference in health effect efficiencies between the CAM-chem and GEOS-Chem models (Figure 1), as CAM-chem simulates relatively more aerosols near the surface compared to the free troposphere across all seasons (Figures S10 and S11).

POA has a more pronounced impact on mortality compared to SOA due to its higher concentration near the surface. VOCs and their oxidized gas products enable SOA formation at locations far from the source and subsequently a broader spatial and vertical extent of SOA (Figures S10−S12). This holds true for SVPOA as well, resulting in a smaller health effect potential of 0.5 million people per Tg year^{-1} for SVPOA (Figure S2b) compared to NVPOA with a health effect potential of 1.1 million people per Tg year^{-1} (Figure 1b). NVPOA and SVPOA exhibit different vertical distributions (Figures S11 and S12), with SVPOA being more prevalent in the free troposphere due to its gas-phase POA tracers and precursors. The oxidation processes also affect the difference between fresh and oxygenated (aged) SVPOA in terms of spatial distribution and health impacts. Fresh SVPOA is restricted to near the surface as a result of its oxidation into oxygenated SVPOA through aging.[37] The resulting health effect of fresh SVPOA is 2.6 million people per Tg year^{-1}, while that of aged SVPOA is 0.4 million people per Tg year^{-1} (Figure S2).

3.2. Aerosol−Radiation Interaction (Direct Effect).

The spatial distribution maps of DRE (Figures S13−S15) generally follow the distribution of aerosol fields (Figures S4−S6), unlike the health effects, where the population is another factor determining the spatial distribution. We calculate global mean all-sky DRE values of −0.44 and −0.36 W m^{-2} for sulfate in GEOS-Chem and CAM-chem, respectively, and −0.51 and −0.37 W m^{-2} for OA in these models. These results are within the ranges reported by previous studies, such as Heald et al.[18] (−0.35 and −0.42 W m^{-2} for sulfate and OA), Yang et al.[103] (−0.42 W m^{-2} for sulfate), and Shrivastava et al.[104] (−0.32 to −0.56 W m^{-2} for OA). Our clear-sky DRE values are also comparable to those in the previous studies, for example, OA DRE of −0.68 and −0.64 W m^{-2} for GEOS-Chem and CAM-chem, respectively, compared to −0.69 W m^{-2} reported by Jo et al.[105]

https://doi.org/10.1021/acs.est.3c02823
Environ. Sci. Technol. 2023, 57, 13793−13807

Figure 2 also shows that the distribution of aerosols with the latitude is proportional to the distribution of DRE with the latitude. CAM-chem shows narrower distributions near the tropics compared to GEOS-Chem, primarily due to differences in biogenic SOA. This is attributed to the stronger formation and faster removal in the SOA scheme used in CAM-chem following the approach by Hodzic et al.[28]

In contrast to the high efficiency of anthropogenic OAs in terms of health impacts, anthropogenic OAs have the lowest efficiency for DRE (Figure 1). In addition, SOA generally has a higher DRE efficiency than POA in CAM-chem. This is because all POA is treated as hydrophobic for DRE calculations in CAM-chem, while only a small fraction of POA is considered hydrophobic in GEOS-Chem (OCPO tracer; Section 2.1). For the same reason, fresh semivolatile POA is less efficient than aged semivolatile POA (Figure S2), as the former is considered hydrophobic while the latter is considered hydrophilic in GEOS-Chem. Marine POA has the highest efficiency in GEOS-Chem, as it primarily distributes over oceanic regions with high relative humidity and hygroscopic growth, consistent with findings from another GEOS-Chem study.[106]

The spatial distributions of OA and their corresponding relative humidity values cannot fully explain the differences in DRE efficiencies between anthropogenic and other (biomass burning and biogenic) sources. For example, anthropogenic POA shows lower DRE efficiencies compared to biomass burning POA in both models, even though the hygroscopicities of anthropogenic and biomass burning POA are the same. Like the calculations for health effects, interannual variability does not significantly influence these differences, with coefficients of variation of less than 4% for all OA categories. This difference is not due to differences in aerosol properties, such as single scattering albedo and asymmetry parameters, as we are investigating the same type of aerosol in this study. Instead, even with the same aerosol loading and meteorological conditions, the surface albedo and solar zenith angle can have a substantial impact on the DRE (including its sign).[106,107]

To disentangle aerosol effects and other conditions, we perform an offline radiative transfer calculation using the column version of RRTMG. With the AOD and other aerosol-related variables kept constant, the DRE is calculated based on the hourly CAM-chem output (meteorological fields) for each month and grid cell, as shown in Figure S16. The offline RRTMG calculation with a constant AOD demonstrates that the DRE varies substantially based on the location and season due to changes in the solar zenith angle and surface albedo. The absolute magnitude of DRE is greater in summer but decreases in winter, which reduces the impact of anthropogenic OA. We do not further distinguish the effects of the solar zenith angle and surface albedo, as the latter is dependent on the former.[108] To further quantify the impact, we use the DRE fields from Figure S16 and calculate the global mean DRE by weighting the spatial distribution of each OA (Figure S17), revealing a higher DRE potential for biogenic and biomass burning OA.

3.3. Aerosol−Cloud Interaction (Indirect Effect).

Figure 3 illustrates the global mean cloud radiative effect changes and efficiencies (per burden) by anthropogenic, biomass burning, biogenic, and all OA for five-year averages of 2010−2014. The cloud radiative effect change efficiency by all OA is calculated to be −1.02 W m^{-2} Tg^{-1} (and −0.22 W m^{-2} Tg^{-1} for DRE efficiency by all OA). Although it is not directly comparable, these values align with the effective radiative forcing (2014−1850) per OA burden according to a recent multimodel comparison study,[109] which ranges between −0.35 and −1.42 W m^{-2} Tg^{-1}. The ranges of interannual variability for changes in cloud radiative effects due to anthropogenic, biomass burning, biogenic, and all OA are −0.49 to −0.53, −0.67 to −0.72, −0.20 to −0.22, and −1.58 to −1.74 W m^{-2}, respectively. These ranges show that the interannual variability does not influence the main conclusions of this study, which are discussed below.

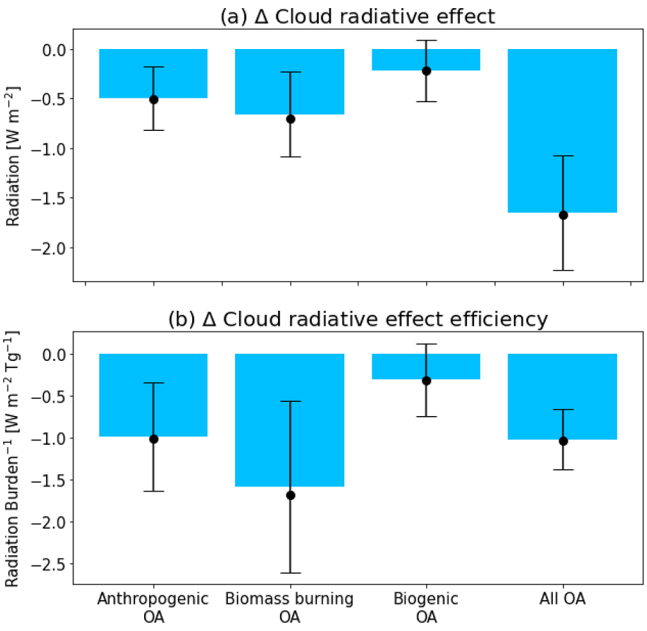

Figure 3. (a) Global mean aerosol indirect effect (W m^{-2}) and (b) aerosol indirect effect efficiency (W m^{-2} Tg^{-1}) simulated by CAM-chem for 2010−2014. The median values are represented by black circles, while the whiskers indicate the one standard deviation range based on 25 h interval output. The aerosol indirect effect is calculated by subtracting the cloud radiative effects from each OA category (anthropogenic, biomass burning, biogenic, and all OA) from the base case results. The aerosol indirect effect efficiency is determined by dividing the aerosol indirect effect by the atmospheric burden.

This analysis presents two main findings. First, biomass burning OA has the greatest potential among the three sources, particularly in high-latitude regions (∼60°) in both hemispheres, where the base cloud radiative effects are substantial (Figure 4). However, the factors contributing to the high aerosol indirect effects of biomass burning OA vary in the two hemispheres. Direct emissions from biomass burning contribute to the effect around 60°N (Figure S4 shows sources in Canada and Russia) while no emission sources due to lower land mass around 60°S.

Global 2D maps reveal that biomass burning OA has a widespread impact throughout the Southern Ocean region in CAM-Chem (Figure S18). In this clean environment, even a small increase in aerosol loading can greatly affect cloud properties compared to a polluted environment.[110] It is noteworthy that the nudged versions of CAM6 were found to reproduce the cloud fraction, cloud phase, and boundary layer structure in the Southern Ocean.[111] Furthermore, CAM-chem with the MAM4 scheme showed good agreement with aircraft measurements of Aitken and accumulation mode number concentrations over the Pacific and Atlantic oceans.[61]

https://doi.org/10.1021/acs.est.3c02823
Environ. Sci. Technol. 2023, 57, 13793−13807

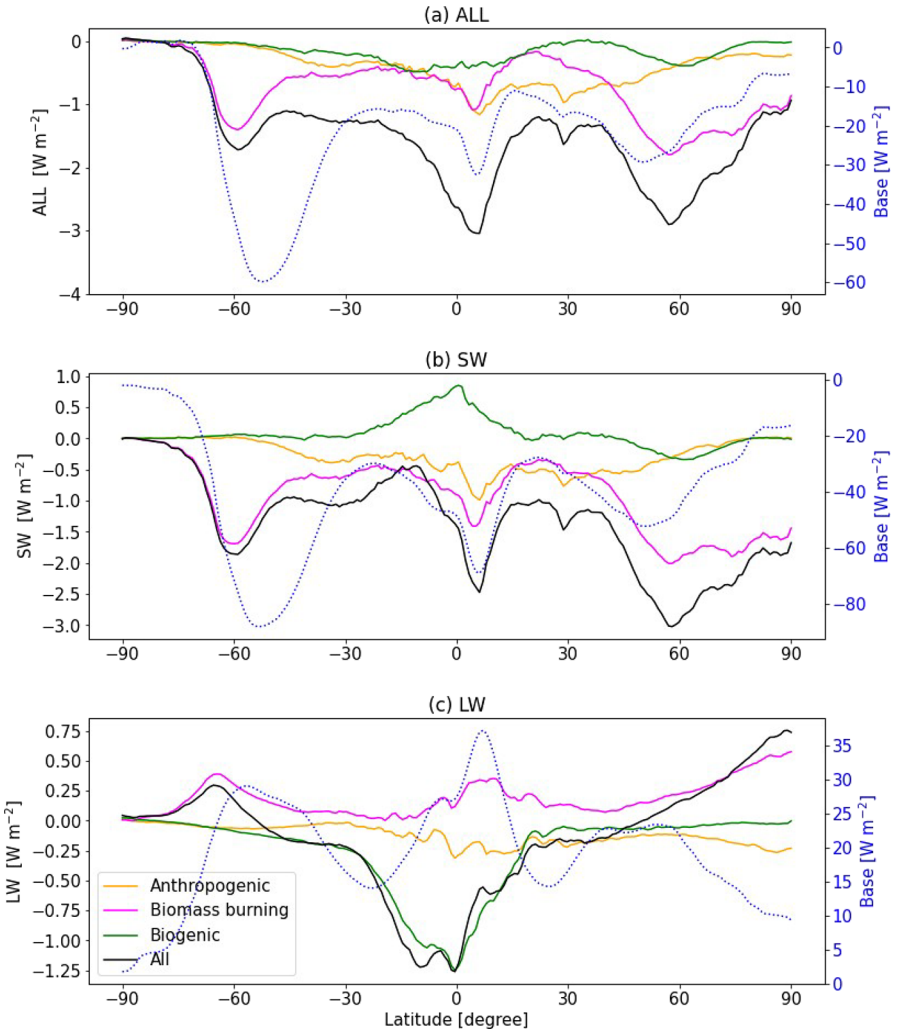

Figure 4. Zonal averages of cloud radiative effect changes by different OA sources. (a) Combined shortwave and longwave, (b) shortwave, and (c) longwave. The values shown represent the difference in radiative effects calculated by subtracting the results of a sensitivity run without each aerosol type from the results of the base run. The results from the base run are shown as blue dotted lines.

The increase in the cloud radiative effect in this region caused by biomass burning OA appears to be strongly linked to the increase in the column-integrated cloud water path, as shown in Figure S19.

Biomass burning OA tends to be present in the free troposphere, with relatively higher values than other OAs from the surface to around 600−700 hPa (Figure S10), which enables their transport to higher latitudes by large-scale circulation. Figure S20 further confirms the transport of biomass burning OA by large-scale motion around 200−300 hPa. The longer lifetime of biomass burning OA compared to other OAs also contributes to their ability to be transported over long distances. The average lifetimes of anthropogenic, biomass burning, and biogenic OAs are calculated as 3.5, 4.9, and 2.8 days, respectively (Table S1).

Biogenic OA has the lowest cooling effect per unit mass, as it does not significantly contribute to cooling in regions where it is abundant. The sign of the indirect effect of biogenic OA can even vary by day and time, as revealed by the one-standard deviation ranges in Figure 3. Biogenic OA has positive shortwave cloud radiative effect changes in regions like Africa and South America near the Amazon (Figure S18). The impact of biogenic OA on the cloud radiative effect differs from the effect of biomass burning OA, as the latter is primarily driven by changes in microphysics, while the former is mainly due to changes in radiation and consequent convective motion.

Specifically, the model simulates reduced updraft and high-level clouds due to biogenic OA over northern South America (Figure S21). Biogenic OA is responsible for the majority of the atmospheric solar heating rate due to aerosols above 400 hPa in this region (Figure S21d). Although biogenic OA mostly scatters sunlight rather than absorbing it, its dominant contribution to the total aerosol mass makes biogenic SOA the most important aerosol for heating as well.

Furthermore, it has the highest cooling effect through aerosol−radiation interaction, with a DRE value of −2.2 W m^{-2} compared to −0.1 and −0.6 W m^{-2} for anthropogenic and biomass burning OA, respectively. This warming in the upper troposphere and cooling at the surface can lead to a more stable atmospheric profile and a decrease in high-level clouds. This, in turn, leads to strong positive shortwave and negative longwave effects, as there is less cloud to reflect solar radiation and trap outgoing longwave radiation. Similarly, a theoretical and observational study by Koren et al.[112] showed that radiative processes can reduce the cloud fraction as AOD increases when AOD is higher than ∼0.2 (Figure 2 in their

https://doi.org/10.1021/acs.est.3c02823
Environ. Sci. Technol. 2023, 57, 13793−13807

paper). Our model analysis of the relationship between simulated AOD, cloud fraction, and convective available potential energy (CAPE) supports these observational findings, the decrease in the cloud fraction and reduction in convective motion as AOD increases when AOD is higher than ~0.2 (Figure S22).

4. DISCUSSION AND IMPLICATIONS

A limitation of this study is that it assumes uniform characteristics for all OA sources, despite using different VBS parameters to simulate the OA concentration. That is, the health and physical characteristics (e.g., toxicity, refractive index, and cloud activation) of OA used in calculating health and climate effects remain the same across all sources. However, this study highlights substantial variations in health and climate impact potential among OA sources, as a result of differences in formation pathways, seasonalities, and spatial and vertical distributions.

The findings of this study can provide valuable insights that inform future research. For example, Pye et al.[113] found that the mortality rate per unit mass of SOA is 6.5 times higher than that of $PM_{2.5}$ at the surface. However, combining with the efficiency (health effects per atmospheric burden) estimated in this study would result in a lower mortality rate of SOA because SOA is more likely to be spread above the boundary layer and spatially beyond the source regions. Our results also indicate that SVPOA has a lower impact on mortality compared to NVPOA due to its volatility, which decreases its overall burden and allows for more efficient transport. Therefore, in future health effect modeling studies, it is important to consider how POA is treated as either semivolatile or nonvolatile in the analysis.

Anthropogenic OA was calculated to have the lowest DRE efficiency, while biomass burning OA has similar or slightly higher DRE efficiency compared to biogenic OA in this study. However, it is worth noting that some fractions of anthropogenic and biomass burning OAs can effectively absorb solar radiation (i.e., brown carbon),[114−116] making biogenic OA potentially the most effective in terms of DRE. The potential of brown carbon absorption to offset the negative DRE by OA greatly varies across studies. An earlier modeling study[117] suggested that brown carbon may change the sign of global OA DRE from a cooling effect (-0.08 W m^{-2}) to a warming effect (0.025 W m^{-2}) in their strongly absorbing brown carbon scenario, but this was based on a simple assumption assigning 92% of biomass and biofuel burning OA as brown carbon. Jo et al.[105] explicitly calculated brown carbon from biomass burning and anthropogenic SOA and showed that brown carbon reduced the OA DRE by 16%. With the incorporation of the photobleaching process in subsequent model studies,[118,119] an observationally constrained global modeling study[120] showed that the DRE of brown carbon was 0.048 W m^{-2}. On the other hand, as biogenic emissions are predicted to increase in the future under all Shared Socioeconomic Pathway (SSP) scenarios,[62] the DRE by biogenic OA may become increasingly important.

The uncertainty in the aerosol−cloud interaction component of global anthropogenic radiative forcing is the largest,[6,121] leading to uncertainties in the magnitude of the indirect effects of OA calculated in this study. CESM2 simulates the largest effective radiative forcing due to aerosol−cloud interaction among the models that participated in the IPCC sixth assessment report.[6] Gettelman et al.[122] reported that CESM2 simulated -1.9 W m^{-2} of cloud radiative effect changes due to aerosol changes between present (2000) and preindustrial (1850) emissions. By comparison, a recent observation-based study[123] calculated radiative forcing due to aerosol−cloud interaction as -1.14 W m^{-2}. Therefore, our estimation of cloud radiative effect changes due to different OA can be considered an upper bound. It is also noteworthy that the radiative effects in this study are calculated with and without each type of OA, which differs from radiative forcing based on the difference between present and preindustrial conditions.

On the other hand, the relative importance of the aerosol indirect effects of anthropogenic, biomass burning, and biogenic OA is more robustly estimated in this study. Combining POA and SOA to estimate their indirect effect helps to alleviate the limitations of the model regarding the POA/SOA ratio discussed in the introduction as well. Biogenic OA has the least efficiency due to changes in radiative effects and convective motion, which is also supported by observational evidence.[112] Biomass burning OA has the highest potential for aerosol indirect effects because it can be transported to remote areas of the atmosphere, where the cloud radiative effect is high and the cloud condensation nuclei (CCN) concentration is low. Strong vertical transport from biomass burning emissions and long-range transport over the Southern hemisphere was also observed from a satellite.[124] Aircraft measurements from a recent field campaign (the NASA Atmospheric Tomography Mission; ATom) reported that biomass burning particles account for one-quarter of the accumulation mode aerosol number in the remote troposphere,[125] which is significant given the low CCN concentration in these regions. The OA scheme used in CAM-chem in this study has been demonstrated to significantly improve OA simulations in these regions.[26] However, the organic-driven nucleation process, which is not yet represented in global models,[126] can be another source of CCN in the remote atmosphere, and biogenic VOCs may play a role in this process.[127] Further development for this process will be needed for a better representation of clouds in models.

The majority of simulations conducted by the Coupled Model Intercomparison Project (CMIP) Phase 5[128] and Phase 6[39] either model the concentration of SOA by applying a fixed yield to emissions or prescribe it, with only a limited number of models explicitly simulating the semivolatile characteristics of SOA through methods like the two-product or VBS approach. This can result in similar distributions of SOA and POA. This study highlights that even when POA and SOA come from the same source, they have different health and radiative effects due to differences in their spatial and vertical distributions and lifetimes. Therefore, for accurate calculation of the radiation field and climate impact in future CMIP phase climate assessments, it is important to either explicitly model the atmospheric processes and chemistry of SOA or apply parameterizations that reflect the influence of key physicochemical drivers of SOA.[129]

Furthermore, half of the CMIP6 models prescribe biogenic VOC emissions,[39] but changes in biogenic emissions and biogenic SOA may play an important role in the radiative budget in the future, as revealed in this study. This is also important in terms of radiative forcing (the difference in radiative effects between present and preindustrial conditions), which is the primary focus of CMIP analyses and IPCC assessments for policy decisions. Therefore, an online coupled

https://doi.org/10.1021/acs.est.3c02823
Environ. Sci. Technol. 2023, 57, 13793−13807

biogenic emission scheme will be necessary for the next generation of CMIP models.

■ ASSOCIATED CONTENT

Supporting Information

The Supporting Information is available free of charge at https://pubs.acs.org/doi/10.1021/acs.est.3c02823.

Additional table (Table S1) and figures (Figures S1−S22) on the global burden and lifetime of OAs simulated by the models, premature death calculated by the GEMM method, clear-sky DRE, semivolatile POA results, global 2D maps for health and climate effects (direct and indirect), vertical distributions of OA with time and latitude, offline RRTMG results, and the relationships between AOD and cloud and CAPE over South America (PDF)

■ AUTHOR INFORMATION

Corresponding Author

Duseong S. Jo − *Atmospheric Chemistry Observations and Modeling Laboratory, National Center for Atmospheric Research, Boulder, Colorado 80301, United States;* orcid.org/0000-0002-7794-1277; Email: cdswk@ucar.edu

Authors

Benjamin A. Nault − *Center for Aerosols and Cloud Chemistry, Aerodyne Research, Inc., Billerica, Massachusetts 01821, United States; Department of Environmental Health and Engineering, The Johns Hopkins University, Baltimore, Maryland 21205, United States;* orcid.org/0000-0001-9464-4787

Simone Tilmes − *Atmospheric Chemistry Observations and Modeling Laboratory, National Center for Atmospheric Research, Boulder, Colorado 80301, United States*

Andrew Gettelman − *Atmospheric Chemistry Observations and Modeling Laboratory, National Center for Atmospheric Research, Boulder, Colorado 80301, United States; Climate and Global Dynamics Laboratory, National Center for Atmospheric Research, Boulder, Colorado 80305, United States;* Present Address: Now at Pacific Northwest National Laboratory, Richland, Washington 99354, United States (A.G.)

Christina S. McCluskey − *Climate and Global Dynamics Laboratory, National Center for Atmospheric Research, Boulder, Colorado 80305, United States*

Alma Hodzic − *Atmospheric Chemistry Observations and Modeling Laboratory, National Center for Atmospheric Research, Boulder, Colorado 80301, United States*

Daven K. Henze − *Department of Mechanical Engineering, University of Colorado Boulder, Boulder, Colorado 80309, United States*

Muhammad Omar Nawaz − *Department of Mechanical Engineering, University of Colorado Boulder, Boulder, Colorado 80309, United States;* Present Address: Now at Department of Environmental and Occupational Health, Milken Institute School of Public Health, George Washington University, Washington, D.C. 20037, United States (M.O.N.).

Ka Ming Fung − *Department of Civil and Environmental Engineering, Massachusetts Institute of Technology, Cambridge, Massachusetts 02139, United States;* orcid.org/0000-0002-7416-2534

Jose L. Jimenez − *Department of Chemistry and Cooperative Institute for Research in Environmental Sciences, University of Colorado Boulder, Boulder, Colorado 80309, United States;* orcid.org/0000-0001-6203-1847

Complete contact information is available at: https://pubs.acs.org/10.1021/acs.est.3c02823

Author Contributions

D.S.J. and J.L.J. conceived the study. D.S.J., B.A.N., S.T., A.H., and J.L.J. developed and implemented organic aerosol schemes used in this study. D.S.J., A.G., C.S.M., and K.M.F. conducted model simulations. D.S.J., D.K.H., and M.O.N. calculated health effects. D.S.J. wrote the manuscript. All authors reviewed and edited the paper.

Funding

This material is based upon work supported by the National Center for Atmospheric Research, which is a major facility sponsored by the National Science Foundation (NSF) under Cooperative Agreement No. 1852977. D.S.J. and J.L.J. were supported by NASA 80NSSC21K1451. D.S.J. and J.L.J. were also supported by NASA 80NSSC21K1439 and NSF AGS 2206655, respectively. B.A.N. was supported by NASA 80NSSC22K0283. K.M.F. was supported by DOE (grant DE-SC0018934). M.O.N. and D.K.H. were supported by NASA NNH17ZDA001N-HAQ.

Notes

The authors declare no competing financial interest.

■ ACKNOWLEDGMENTS

We would like to acknowledge high-performance computing support from Cheyenne (doi: 10.5065/D6RX99HX) provided by NCAR's Computational and Information Systems Laboratory, sponsored by the NSF. We thank Louisa K. Emmons for her valuable contributions and support to the manuscript. We also thank Wenfu Tang and Rebecca R. Buchholz for their helpful comments on the manuscript.

■ REFERENCES

(1) Founda, D.; Kazadzis, S.; Mihalopoulos, N.; Gerasopoulos, E.; Lianou, M.; Raptis, P. I. Long-Term Visibility Variation in Athens (1931−2013): A Proxy for Local and Regional Atmospheric Aerosol Loads. *Atmos. Chem. Phys.* **2016**, *16*, 11219−11236.

(2) Jo, D. S.; Park, R. J.; Kim, M. J.; Spracklen, D. V. Effects of chemical aging on global secondary organic aerosol using the volatility basis set approach. *Atmos. Environ.* **2013**, *81*, 230−244.

(3) Glotfelty, T.; He, J.; Zhang, Y. Improving Organic Aerosol Treatments in CESM/CAM5: Development, Application, and Evaluation. *J. Adv. Model Earth Syst.* **2017**, *9*, 1506−1539.

(4) Shiraiwa, M.; Ueda, K.; Pozzer, A.; Lammel, G.; Kampf, C. J.; Fushimi, A.; Enami, S.; Arangio, A. M.; Fröhlich-Nowoisky, J.; Fujitani, Y.; Furuyama, A.; Lakey, P. S. J.; Lelieveld, J.; Lucas, K.; Morino, Y.; Pöschl, U.; Takahama, S.; Takami, A.; Tong, H.; Weber, B.; Yoshino, A.; Sato, K. Aerosol Health Effects from Molecular to Global Scales. *Environ. Sci. Technol.* **2017**, *51*, 13545−13567.

(5) Brasseur, G. P.; Jacob, D. J. *Modeling of Atmospheric Chemistry*; Cambridge University Press: Cambridge, 2017, DOI: 10.1017/9781316544754.

(6) Forster, P., Storelvmo, T., Armour, K., Collins, W., Dufresne, J. L., Frame, D., Lunt, D. J., Mauritsen, T., Palmer, M. D., Watanabe, M., Wild, M., Zhang, H. The Earth's Energy Budget, Climate Feedbacks and Climate Sensitivity. In *Climate Change 2021: The Physical Science Basis. Contribution of Working Group I to the Sixth Assessment Report of*

the Intergovernmental Panel on Climate Change; Masson-Delmotte, V., Zhai, P., Pirani, A., Connors, S. L., Péan, C., Berger, S., Caud, N., Chen, Y., Goldfarb, L., Gomis, M. I., Huang, M., Leitzell, K., Lonnoy, E., Matthews, J. B. R., Maycock, T. K., Waterfield, T., Yelekçi, O., Yu, R., Zhou, B., Ed.; Cambridge University Press: Cambridge, United Kingdom and New York, NY, USA, *2021*; pp. 923−1054.

(7) Zhang, Q.; Jimenez, J. L.; Canagaratna, M. R.; Allan, J. D.; Coe, H.; Ulbrich, I.; Alfarra, M. R.; Takami, A.; Middlebrook, A. M.; Sun, Y. L.; Dzepina, K.; Dunlea, E.; Docherty, K.; DeCarlo, P. F.; Salcedo, D.; Onasch, T.; Jayne, J. T.; Miyoshi, T.; Shimono, A.; Hatakeyama, S.; Takegawa, N.; Kondo, Y.; Schneider, J.; Drewnick, F.; Borrmann, S.; Weimer, S.; Demerjian, K.; Williams, P.; Bower, K.; Bahreini, R.; Cottrell, L.; Griffin, R. J.; Rautiainen, J.; Sun, J. Y.; Zhang, Y. M.; Worsnop, D. R. Ubiquity and Dominance of Oxygenated Species in Organic Aerosols in Anthropogenically-Influenced Northern Hemisphere Midlatitudes. *Geophys. Res. Lett.* **2007**, *34* (), DOI: 10.1029/2007gl029979.

(8) Heald, C. L.; Jacob, D. J.; Park, R. J.; Russell, L. M.; Huebert, B. J.; Seinfeld, J. H.; Liao, H.; Weber, R. J. A Large Organic Aerosol Source in the Free Troposphere Missing from Current Models. *Geophys. Res. Lett.* **2005**, *32*, 1−4.

(9) Volkamer, R.; Jimenez, J. L.; San Martini, F.; Dzepina, K.; Zhang, Q.; Salcedo, D.; Molina, L. T.; Worsnop, D. R.; Molina, M. J. Secondary organic aerosol formation from anthropogenic air pollution: Rapid and higher than expected. *Geophys. Res. Lett.* **2006**, *33*, 4407.

(10) Tsigaridis, K.; Daskalakis, N.; Kanakidou, M.; Adams, P. J.; Artaxo, P.; Bahadur, R.; Balkanski, Y.; Bauer, S. E.; Bellouin, N.; Benedetti, A.; Bergman, T.; Berntsen, T. K.; Beukes, J. P.; Bian, H.; Carslaw, K. S.; Chin, M.; Curci, G.; Diehl, T.; Easter, R. C.; Ghan, S. J.; Gong, S. L.; Hodzic, A.; Hoyle, C. R.; Iversen, T.; Jathar, S.; Jimenez, J. L.; Kaiser, J. W.; Kirkevåg, A.; Koch, D.; Kokkola, H.; Lee, Y. H.; Lin, G.; Liu, X.; Luo, G.; Ma, X.; Mann, G. W.; Mihalopoulos, N.; Morcrette, J.-J.; Müller, J.-F.; Myhre, G.; Myriokefalitakis, S.; Ng, N. L.; O'Donnell, D.; Penner, J. E.; Pozzoli, L.; Pringle, K. J.; Russell, L. M.; Schulz, M.; Sciare, J.; Seland, Ø.; Shindell, D. T.; Sillman, S.; Skeie, R. B.; Spracklen, D.; Stavrakou, T.; Steenrod, S. D.; Takemura, T.; Tiitta, P.; Tilmes, S.; Tost, H.; van Noije, T.; van Zyl, P. G.; von Salzen, K.; Yu, F.; Wang, Z.; Zaveri, R. A.; Zhang, H.; Zhang, K.; Zhang, Q.; Zhang, X. The AeroCom evaluation and intercomparison of organic aerosol in global models. *Atmos. Chem. Phys.* **2014**, *14*, 10845−10895.

(11) Goldstein, A. H.; Galbally, I. E. Known and unexplored organic constituents in the earth's atmosphere. *Environ. Sci. Technol.* **2007**, *41*, 1514−1521.

(12) Szopa, S.; Naik, V.; Adhikary, B.; Artaxo, P.; Berntsen, T.; Collins, W. D.; Fuzzi, S.; Gallardo, L.; Kiendler-Scharr, A.; Klimont, Z.; Liao, H.; Unger, N.; Zanis, P. Short-Lived Climate Forcers. In *Climate Change 2021: The Physical Science Basis. Contribution of Working Group I to the Sixth Assessment Report of the Intergovernmental Panel on Climate Change*; Masson-Delmotte, V., Zhai, P., Pirani, A., Connors, S. L., Péan, C., Berger, S., Caud, N., Chen, Y., Goldfarb, L., Gomis, M. I., Huang, M., Leitzell, K., Lonnoy, E., Matthews, J. B. R., Maycock, T. K., Waterfield, T., Yelekçi, O., Yu, R., Zhou, B., Eds.; Cambridge University Press: Cambridge, United Kingdom and New York, NY, USA, *2021*; pp. 817−922.

(13) Shindell, D.; Smith, C. J. Climate and Air-Quality Benefits of a Realistic Phase-out of Fossil Fuels. *Nature* **2019**, *573*, 408−411.

(14) Hallquist, M.; Wenger, J. C.; Baltensperger, U.; Rudich, Y.; Simpson, D.; Claeys, M.; Dommen, J.; Donahue, N. M.; George, C.; Goldstein, A. H.; Hamilton, J. F.; Herrmann, H.; Hoffmann, T.; Iinuma, Y.; Jang, M.; Jenkin, M. E.; Jimenez, J. L.; Kiendler-Scharr, A.; Maenhaut, W.; McFiggans, G.; Mentel, T. F.; Monod, A.; Prévôt, A. S. H.; Seinfeld, J. H.; Surratt, J. D.; Szmigielski, R.; Wildt, J. The formation, properties and impact of secondary organic aerosol: current and emerging issues. *Atmos. Chem. Phys.* **2009**, *9*, 5155−5236.

(15) Kanakidou, M.; Seinfeld, J. H.; Pandis, S. N.; Barnes, I.; Dentener, F. J.; Facchini, M. C.; Van Dingenen, R.; Ervens, B.; Nenes, A.; Nielsen, C. J.; Swietlicki, E.; Putaud, J. P.; Balkanski, Y.; Fuzzi, S.; Horth, J.; Moortgat, G. K.; Winterhalter, R.; Myhre, C. E. L.; Tsigaridis, K.; Vignati, E.; Stephanou, E. G.; Wilson, J. Organic aerosol and global climate modelling: a review. *Atmos. Chem. Phys.* **2005**, *5*, 1053−1123.

(16) Nault, B. A.; Jo, D. S.; McDonald, B. C.; Campuzano-Jost, P.; Day, D. A.; Hu, W.; Schroder, J. C.; Allan, J.; Blake, D. R.; Canagaratna, M. R.; Coe, H.; Coggon, M. M.; DeCarlo, P. F.; Diskin, G. S.; Dunmore, R.; Flocke, F.; Fried, A.; Gilman, J. B.; Gkatzelis, G.; Hamilton, J. F.; Hanisco, T. F.; Hayes, P. L.; Henze, D. K.; Hodzic, A.; Hopkins, J.; Hu, M.; Huey, L. G.; Jobson, B. T.; Kuster, W. C.; Lewis, A.; Li, M.; Liao, J.; Nawaz, M. O.; Pollack, I. B.; Peischl, J.; Rappenglück, B.; Reeves, C. E.; Richter, D.; Roberts, J. M.; Ryerson, T. B.; Shao, M.; Sommers, J. M.; Walega, J.; Warneke, C.; Weibring, P.; Wolfe, G. M.; Young, D. E.; Yuan, B.; Zhang, Q.; de Gouw, J. A.; Jimenez, J. L. Secondary Organic Aerosols from Anthropogenic Volatile Organic Compounds Contribute Substantially to Air Pollution Mortality. *Atmos. Chem. Phys.* **2021**, *21*, 11201−11224.

(17) Chowdhury, S.; Pozzer, A.; Haines, A.; Klingmüller, K.; Münzel, T.; Paasonen, P.; Sharma, A.; Venkataraman, C.; Lelieveld, J. Global Health Burden of Ambient PM2.5 and the Contribution of Anthropogenic Black Carbon and Organic Aerosols. *Environ. Int.* **2022**, *159*, No. 107020.

(18) Heald, C. L.; Ridley, D. A.; Kroll, J. H.; Barrett, S. R. H.; Cady-Pereira, K. E.; Alvarado, M. J.; Holmes, C. D. Contrasting the direct radiative effect and direct radiative forcing of aerosols. *Atmos. Chem. Phys.* **2014**, *14*, 5513−5527.

(19) Spracklen, D. V.; Jimenez, J. L.; Carslaw, K. S.; Worsnop, D. R.; Evans, M. J.; Mann, G. W.; Zhang, Q.; Canagaratna, M. R.; Allan, J.; Coe, H.; McFiggans, G.; Rap, A.; Forster, P. Aerosol mass spectrometer constraint on the global secondary organic aerosol budget. *Atmos. Chem. Phys.* **2011**, *11*, 12109−12136.

(20) Sporre, M. K.; Blichner, S. M.; Schrödner, R.; Karset, I. H. H.; Berntsen, T. K.; van Noije, T.; Bergman, T.; O'Donnell, D.; Makkonen, R. Large Difference in Aerosol Radiative Effects from BVOC-SOA Treatment in Three Earth System Models. *Atmos. Chem. Phys.* **2020**, *20*, 8953−8973.

(21) Shrivastava, M.; Cappa, C. D.; Fan, J.; Goldstein, A. H.; Guenther, A. B.; Jimenez, J. L.; Kuang, C.; Laskin, A.; Martin, S. T.; Ng, N. L.; Petaja, T.; Pierce, J. R.; Rasch, P. J.; Roldin, P.; Seinfeld, J. H.; Shilling, J.; Smith, J. N.; Thornton, J. A.; Volkamer, R.; Wang, J.; Worsnop, D. R.; Zaveri, R. A.; Zelenyuk, A.; Zhang, Q. Recent Advances in Understanding Secondary Organic Aerosol: Implications for Global Climate Forcing: Advances in Secondary Organic Aerosol. *Rev. Geophys.* **2017**, *55*, 509−559.

(22) Mei, F.; Hayes, P. L.; Ortega, A.; Taylor, J. W.; Allan, J. D.; Gilman, J.; Kuster, W.; de Gouw, J.; Jimenez, J. L.; Wang, J. Droplet Activation Properties of Organic Aerosols Observed at an Urban Site during CalNex-LA. *J. Geophys. Res.* **2013**, *118*, 2903−2917.

(23) Mei, F.; Setyan, A.; Zhang, Q.; Wang, J. CCN Activity of Organic Aerosols Observed Downwind of Urban Emissions during CARES. *Atmos. Chem. Phys.* **2013**, *13*, 12155−12169.

(24) Levin, E. J. T.; Prenni, A. J.; Palm, B. B.; Day, D. A.; Campuzano-Jost, P.; Winkler, P. M.; Kreidenweis, S. M.; DeMott, P. J.; Jimenez, J. L.; Smith, J. N. Size-Resolved Aerosol Composition and Its Link to Hygroscopicity at a Forested Site in Colorado. *Atmos. Chem. Phys.* **2014**, *14*, 2657−2667.

(25) Pai, S. J.; Heald, C. L.; Pierce, J. R.; Farina, S. C.; Marais, E. A.; Jimenez, J. L.; Campuzano-Jost, P.; Nault, B. A.; Middlebrook, A. M.; Coe, H.; Shilling, J. E.; Bahreini, R.; Dingle, J. H.; Vu, K. An Evaluation of Global Organic Aerosol Schemes Using Airborne Observations. *Atmos. Chem. Phys.* **2020**, *20*, 2637−2665.

(26) Hodzic, A.; Campuzano-Jost, P.; Bian, H.; Chin, M.; Colarco, P. R.; Day, D. A.; Froyd, K. D.; Heinold, B.; Jo, D. S.; Katich, J. M.; Kodros, J. K.; Nault, B. A.; Pierce, J. R.; Ray, E.; Schacht, J.; Schill, G. P.; Schroder, J. C.; Schwarz, J. P.; Sueper, D. T.; Tegen, I.; Tilmes, S.; Tsigaridis, K.; Yu, P.; Jimenez, J. L. Characterization of Organic Aerosol across the Global Remote Troposphere: A Comparison of ATom Measurements and Global Chemistry Models. *Atmos. Chem. Phys.* **2020**, *20*, 4607−4635.

(27) Marais, E. A.; Jacob, D. J.; Jimenez, J. L.; Campuzano-Jost, P.; Day, D. A.; Hu, W.; Krechmer, J.; Zhu, L.; Kim, P. S.; Miller, C. C.; Fisher, J. A.; Travis, K.; Yu, K.; Hanisco, T. F.; Wolfe, G. M.; Arkinson, H. L.; Pye, H. O. T.; Froyd, K. D.; Liao, J.; McNeill, V. F. Aqueous-Phase Mechanism for Secondary Organic Aerosol Formation from Isoprene: Application to the Southeast United States and Co-Benefit of SO_2 Emission Controls. *Atmos. Chem. Phys.* **2016**, *16*, 1603−1618.
(28) Hodzic, A.; Kasibhatla, P. S.; Jo, D. S.; Cappa, C. D.; Jimenez, J. L.; Madronich, S.; Park, R. J. Rethinking the Global Secondary Organic Aerosol (SOA) Budget: Stronger Production, Faster Removal, Shorter Lifetime. *Atmos. Chem. Phys.* **2016**, *16*, 7917−7941.
(29) Hodzic, A.; Aumont, B.; Knote, C.; Lee-Taylor, J.; Madronich, S.; Tyndall, G. Volatility Dependence of Henry's Law Constants of Condensable Organics: Application to Estimate Depositional Loss of Secondary Organic Aerosols. *Geophys. Res. Lett.* **2014**, *41*, 4795−4804.
(30) Kim, P. S.; Jacob, D. J.; Fisher, J. A.; Travis, K.; Yu, K.; Zhu, L.; Yantosca, R. M.; Sulprizio, M. P.; Jimenez, J. L.; Campuzano-Jost, P.; Froyd, K. D.; Liao, J.; Hair, J. W.; Fenn, M. A.; Butler, C. F.; Wagner, N. L.; Gordon, T. D.; Welti, A.; Wennberg, P. O.; Crounse, J. D.; Clair, J. M. S.; Teng, A. P.; Millet, D. B.; Schwarz, J. P.; Markovic, M. Z.; Perring, A. E. Sources, seasonality, and trends of southeast US aerosol: an integrated analysis of surface, aircraft, and satellite observations with the GEOS-Chem chemical transport model. *Atmos. Chem. Phys.* **2015**, *15*, 10411−10433.
(31) Schroder, J. C.; Campuzano-Jost, P.; Day, D. A.; Shah, V.; Larson, K.; Sommers, J. M.; Sullivan, A. P.; Campos, T.; Reeves, J. M.; Hills, A.; Hornbrook, R. S.; Blake, N. J.; Scheuer, E.; Guo, H.; Fibiger, D. L.; McDuffie, E. E.; Hayes, P. L.; Weber, R. J.; Dibb, J. E.; Apel, E. C.; Jaeglé, L.; Brown, S. S.; Thornton, J. A.; Jimenez, J. L. Sources and Secondary Production of Organic Aerosols in the Northeastern United States during WINTER. *J. Geophys. Res. D: Atmos.* **2018**, *42*, 4478.
(32) Fisher, J. A.; Jacob, D. J.; Travis, K. R.; Kim, P. S.; Marais, E. A.; Miller, C. C.; Yu, K.; Zhu, L.; Yantosca, R. M.; Sulprizio, M. P.; Mao, J.; Wennberg, P. O.; Crounse, J. D.; Teng, A. P.; Nguyen, T. B.; St Clair, J. M.; Cohen, R. C.; Romer, P.; Nault, B. A.; Wooldridge, P. J.; Jimenez, J. L.; Campuzano-Jost, P.; Day, D. A.; Hu, W.; Shepson, P. B.; Xiong, F.; Blake, D. R.; Goldstein, A. H.; Misztal, P. K.; Hanisco, T. F.; Wolfe, G. M.; Ryerson, T. B.; Wisthaler, A.; Mikoviny, T. Organic Nitrate Chemistry and Its Implications for Nitrogen Budgets in an Isoprene- and Monoterpene-Rich Atmosphere: Constraints from Aircraft (SEAC4RS) and Ground-Based (SOAS) Observations in the Southeast US. *Atmos. Chem. Phys.* **2016**, *16*, 5969−5991.
(33) Travis, K. R.; Jacob, D. J.; Fisher, J. A.; Kim, P. S.; Marais, E. A.; Zhu, L.; Yu, K.; Miller, C. C.; Yantosca, R. M.; Sulprizio, M. P.; Thompson, A. M.; Wennberg, P. O.; Crounse, J. D.; St Clair, J. M.; Cohen, R. C.; Laughner, J. L.; Dibb, J. E.; Hall, S. R.; Ullmann, K.; Wolfe, G. M.; Pollack, I. B.; Peischl, J.; Neuman, J. A.; Zhou, X. Why do models overestimate surface ozone in the Southeast United States? *Atmos. Chem. Phys.* **2016**, *16*, 13561−13577.
(34) Tilmes, S.; Hodzic, A.; Emmons, L. K.; Mills, M. J.; Gettelman, A.; Kinnison, D. E.; Park, M.; Lamarque, J. F.; Vitt, F.; Shrivastava, M.; Campuzano-Jost, P.; Jimenez, J. L.; Liu, X. Climate Forcing and Trends of Organic Aerosols in the Community Earth System Model (CESM2). *J. Adv. Model. Earth Syst.* **2019**, *18*, 745.
(35) Kaiser, J.; Jacob, D. J.; Zhu, L.; Travis, K. R.; Fisher, J. A.; González Abad, G.; Zhang, L.; Zhang, X.; Fried, A.; Crounse, J. D.; St Clair, J. M.; Wisthaler, A. High-Resolution Inversion of OMI Formaldehyde Columns to Quantify Isoprene Emission on Ecosystem-Relevant Scales: Application to the Southeast US. *Atmos. Chem. Phys.* **2018**, *18*, 5483−5497.
(36) Oak, Y. J.; Park, R. J.; Jo, D. S.; Hodzic, A.; Jimenez, J. L.; Campuzano-Jost, P.; Nault, B. A.; Kim, H.; Kim, H.; Ha, E. S.; Song, C.-K.; Yi, S.-M.; Diskin, G. S.; Weinheimer, A. J.; Blake, D. R.; Wisthaler, A.; Shim, M.; Shin, Y. Evaluation of Secondary Organic Aerosol (SOA) Simulations for Seoul, Korea. *J. Adv. Model. Earth Syst.* **2022**, *14*, No. e2021MS002760.
(37) Pye, H. O. T.; Seinfeld, J. H. A global perspective on aerosol from low-volatility organic compounds. *Atmos. Chem. Phys.* **2010**, *10*, 4377−4401.
(38) Schwantes, R. H.; Lacey, F. G.; Tilmes, S.; Emmons, L. K.; Lauritzen, P. H.; Walters, S.; Callaghan, P.; Zarzycki, C. M.; Barth, M. C.; Jo, D. S.; Bacmeister, J. T.; Neale, R. B.; Vitt, F.; Kluzek, E.; Roozitalab, B.; Hall, S. R.; Ullmann, K.; Warneke, C.; Peischl, J.; Pollack, I. B.; Flocke, F.; Wolfe, G. M.; Hanisco, T. F.; Keutsch, F. N.; Kaiser, J.; Bui, T. P. V.; Jimenez, J. L.; Campuzano-Jost, P.; Apel, E. C.; Hornbrook, R. S.; Hills, A. J.; Yuan, B.; Wisthaler, A. Evaluating the Impact of Chemical Complexity and Horizontal Resolution on Tropospheric Ozone over the Conterminous US with a Global Variable Resolution Chemistry Model. *J. Adv. Model. Earth Syst.* **2022**, *14*, No. e2021MS002889.
(39) Turnock, S. T.; Allen, R. J.; Andrews, M.; Bauer, S. E.; Deushi, M.; Emmons, L.; Good, P.; Horowitz, L.; John, J. G.; Michou, M.; Nabat, P.; Naik, V.; Neubauer, D.; O'Connor, F. M.; Olivié, D.; Oshima, N.; Schulz, M.; Sellar, A.; Shim, S.; Takemura, T.; Tilmes, S.; Tsigaridis, K.; Wu, T.; Zhang, J. Historical and Future Changes in Air Pollutants from CMIP6 Models. *Atmos. Chem. Phys.* **2020**, *20*, 14547−14579.
(40) Lacagnina, C.; Hasekamp, O. P.; Bian, H.; Curci, G.; Myhre, G.; Noije, T.; Schulz, M.; Skeie, R. B.; Takemura, T.; Zhang, K. Aerosol single-scattering albedo over the global oceans: Comparing PARASOL retrievals with AERONET, OMI, and AeroCom models estimates. *J. Geophys. Res.: Atmos.* **2015**, *120*, 9814−9836.
(41) Myhre, G.; Samset, B. H.; Schulz, M.; Balkanski, Y.; Bauer, S.; Berntsen, T. K.; Bian, H.; Bellouin, N.; Chin, M.; Diehl, T.; et al. Radiative forcing of the direct aerosol effect from AeroCom Phase II simulations. *Atmos. Chem. Phys.* **2013**, *13*, 1853.
(42) Tan, J.; Fu, J. S.; Carmichael, G. R.; Itahashi, S.; Tao, Z.; Huang, K.; Dong, X.; Yamaji, K.; Nagashima, T.; Wang, X.; Liu, Y.; Lee, H.-J.; Lin, C.-Y.; Ge, B.; Kajino, M.; Zhu, J.; Zhang, M.; Liao, H.; Wang, Z. Why Do Models Perform Differently on Particulate Matter over East Asia? A Multi-Model Intercomparison Study for MICS-Asia III. *Atmos. Chem. Phys.* **2020**, *20*, 7393−7410.
(43) Yu, H.; Chin, M.; West, J. J.; Atherton, C. S.; Bellouin, N.; Bergmann, D.; Bey, I.; Bian, H.; Diehl, T.; Forberth, G.; Hess, P.; Schulz, M.; Shindell, D.; Takemura, T.; Tan, Q. A Multimodel Assessment of the Influence of Regional Anthropogenic Emission Reductions on Aerosol Direct Radiative Forcing and the Role of Intercontinental Transport. *J. Geophys. Res.: Atmos.* **2013**, *118*, 700−720.
(44) Dong, X.; Fu, J. S.; Zhu, Q.; Sun, J.; Tan, J.; Keating, T.; Sekiya, T.; Sudo, K.; Emmons, L.; Tilmes, S.; Jonson, J. E.; Schulz, M.; Bian, H.; Chin, M.; Davila, Y.; Henze, D.; Takemura, T.; Benedictow, A. M. K.; Huang, K. Long-Range Transport Impacts on Surface Aerosol Concentrations and the Contributions to Haze Events in China: An HTAP2 Multi-Model Study. *Atmos. Chem. Phys.* **2018**, *18*, 15581−15600.
(45) Stjern, C. W.; Samset, B. H.; Myhre, G.; Bian, H.; Chin, M.; Davila, Y.; Dentener, F.; Emmons, L.; Flemming, J.; Haslerud, A. S.; Henze, D.; Jonson, J. E.; Kucsera, T.; Lund, M. T.; Schulz, M.; Sudo, K.; Takemura, T.; Tilmes, S. Global and Regional Radiative Forcing from 20% Reductions in BC, OC and SO_4 − an HTAP2 Multi-Model Study. *Atmos. Chem. Phys.* **2016**, *16*, 13579−13599.
(46) Mortier, A.; Gliß, J.; Schulz, M.; Aas, W.; Andrews, E.; Bian, H.; Chin, M.; Ginoux, P.; Hand, J.; Holben, B.; Zhang, H.; Kipling, Z.; Kirkevåg, A.; Laj, P.; Lurton, T.; Myhre, G.; Neubauer, D.; Olivié, D.; von Salzen, K.; Skeie, R. B.; Takemura, T.; Tilmes, S. Evaluation of Climate Model Aerosol Trends with Ground-Based Observations over the Last 2 Decades − an AeroCom and CMIP6 Analysis. *Atmos. Chem. Phys.* **2020**, *20*, 13355−13378.
(47) Mann, G. W.; Carslaw, K. S.; Reddington, C. L.; Pringle, K. J.; Schulz, M.; Asmi, A.; Spracklen, D. V.; Ridley, D. A.; Woodhouse, M. T.; Lee, L. A.; Zhang, K.; Ghan, S. J.; Easter, R. C.; Liu, X.; Stier, P.; Lee, Y. H.; Adams, P. J.; Tost, H.; Lelieveld, J.; Bauer, S. E.; Tsigaridis, K.; van Noije, T. P. C.; Strunk, A.; Vignati, E.; Bellouin, N.; Dalvi, M.; Johnson, C. E.; Bergman, T.; Kokkola, H.; von Salzen, K.; Yu, F.; Luo,

https://doi.org/10.1021/acs.est.3c02823
Environ. Sci. Technol. 2023, 57, 13793−13807

G.; Petzold, A.; Heintzenberg, J.; Clarke, A.; Ogren, J. A.; Gras, J.; Baltensperger, U.; Kaminski, U.; Jennings, S. G.; O'Dowd, C. D.; Harrison, R. M.; Beddows, D. C. S.; Kulmala, M.; Viisanen, Y.; Ulevicius, V.; Mihalopoulos, N.; Zdimal, V.; Fiebig, M.; Hansson, H.-C.; Swietlicki, E.; Henzing, J. S. Intercomparison and Evaluation of Global Aerosol Microphysical Properties among AeroCom Models of a Range of Complexity. *Atmos. Chem. Phys.* **2014**, *14*, 4679−4713.

(48) Chen, L.; Gao, Y.; Zhang, M.; Fu, J. S.; Zhu, J.; Liao, H.; Li, J.; Huang, K.; Ge, B.; Wang, X.; Lam, Y. F.; Lin, C.-Y.; Itahashi, S.; Nagashima, T.; Kajino, M.; Yamaji, K.; Wang, Z.; Kurokawa, J.-I. MICS-Asia III: Multi-Model Comparison and Evaluation of Aerosol over East Asia. *Atmos. Chem. Phys.* **2019**, *19*, 11911−11937.

(49) Sand, M.; Samset, B. H.; Balkanski, Y.; Bauer, S.; Bellouin, N.; Berntsen, T. K.; Bian, H.; Chin, M.; Diehl, T.; Easter, R.; Ghan, S. J.; Iversen, T.; Kirkevåg, A.; Lamarque, J.-F.; Lin, G.; Liu, X.; Luo, G.; Myhre, G.; van Noije, T.; Penner, J. E.; Schulz, M.; Seland, Ø.; Skeie, R. B.; Stier, P.; Takemura, T.; Tsigaridis, K.; Yu, F.; Zhang, K.; Zhang, H. Aerosols at the Poles: An AeroCom Phase II Multi-Model Evaluation. *Atmos. Chem. Phys.* **2017**, *17*, 12197−12218.

(50) Bey, I.; Jacob, D. J.; Yantosca, R. M.; Logan, J. A.; Field, B. D.; Fiore, A. M.; Li, Q.; Liu, H. Y.; Mickley, L. J.; Schultz, M. G. Global Modeling of Tropospheric Chemistry with Assimilated Meteorology: Model Description and Evaluation. *J. Geophys. Res.* **2001**, *106*, 23073−23095.

(51) Park, R. J.; Jacob, D. J.; Chin, M.; Martin, R. V. Sources of Carbonaceous Aerosols over the United States and Implications for Natural Visibility. *J. Geophys. Res.: Atmos.* **2003**, *108* (), DOI: 10.1029/2002JD003190.

(52) Gantt, B.; Johnson, M. S.; Crippa, M.; Prévôt, A. S. H.; Meskhidze, N. Implementing Marine Organic Aerosols into the GEOS-Chem Model. *Geosci. Model Dev.* **2015**, *8*, 619−629.

(53) Hodzic, A.; Jimenez, J. L. Modeling anthropogenically controlled secondary organic aerosols in a megacity: A simplified framework for global and climate models. *Geosci. Model Dev.* **2011**, *4*, 901.

(54) McDuffie, E. E.; Martin, R. V.; Spadaro, J. V.; Burnett, R.; Smith, S. J.; O'Rourke, P.; Hammer, M. S.; van Donkelaar, A.; Bindle, L.; Shah, V.; Jaeglé, L.; Luo, G.; Yu, F.; Adeniran, J. A.; Lin, J.; Brauer, M. Source Sector and Fuel Contributions to Ambient PM2.5 and Attributable Mortality across Multiple Spatial Scales. *Nat. Commun.* **2021**, *12*, 3594.

(55) Pye, H. O. T.; Chan, A. W. H.; Barkley, M. P.; Seinfeld, J. H. Global Modeling of Organic Aerosol: The Importance of Reactive Nitrogen (NO_x and NO_3). *Atmos. Chem. Phys.* **2010**, *10*, 11261−11276.

(56) Danabasoglu, G.; Lamarque, J. F.; Bacmeister, J.; Bailey, D. A.; DuVivier, A. K.; Edwards, J.; Emmons, L. K.; Fasullo, J.; Garcia, R.; Gettelman, A.; Hannay, C.; Holland, M. M.; Large, W. G.; Lauritzen, P. H.; Lawrence, D. M.; Lenaerts, J. T. M.; Lindsay, K.; Lipscomb, W. H.; Mills, M. J.; Neale, R.; Oleson, K. W.; Otto-Bliesner, B.; Phillips, A. S.; Sacks, W.; Tilmes, S.; Kampenhout, L.; Vertenstein, M.; Bertini, A.; Dennis, J.; Deser, C.; Fischer, C.; Fox-Kemper, B.; Kay, J. E.; Kinnison, D.; Kushner, P. J.; Larson, V. E.; Long, M. C.; Mickelson, S.; Moore, J. K.; Nienhouse, E.; Polvani, L.; Rasch, P. J.; Strand, W. G. The Community Earth System Model Version 2 (CESM2). *J. Adv. Model. Earth Syst.* **2020**, *12*, No. e2019MS001916.

(57) Emmons, L. K.; Schwantes, R. H.; Orlando, J. J.; Tyndall, G.; Kinnison, D.; Lamarque, J.; Marsh, D.; Mills, M. J.; Tilmes, S.; Bardeen, C.; Buchholz, R. R.; Conley, A.; Gettelman, A.; Garcia, R.; Simpson, I.; Blake, D. R.; Meinardi, S.; Pétron, G. The Chemistry Mechanism in the Community Earth System Model Version 2 (CESM2). *J. Adv. Model. Earth Syst.* **2020**, *12*, No. e2019MS001916.

(58) Liu, X.; Ma, P.-L.; Wang, H.; Tilmes, S.; Singh, B.; Easter, R. C.; Ghan, S. J.; Rasch, P. J. Description and evaluation of a new four-mode version of the Modal Aerosol Module (MAM4) within version 5.3 of the Community Atmosphere Model. *Geosci. Model Dev.* **2016**, *9*, 505−522.

(59) Liu, X.; Easter, R. C.; Ghan, S. J.; Zaveri, R.; Rasch, P.; Shi, X.; Lamarque, J.-F.; Gettelman, A.; Morrison, H.; Vitt, F.; Conley, A.; Park, S.; Neale, R.; Hannay, C.; Ekman, A. M. L.; Hess, P.; Mahowald, N.; Collins, W.; Iacono, M. J.; Bretherton, C. S.; Flanner, M. G.; Mitchell, D. Toward a minimal representation of aerosols in climate models: description and evaluation in the Community Atmosphere Model CAM5. *Geosci. Model Dev.* **2012**, *5*, 709−739.

(60) Vehkamäki, H.; Kulmala, M.; Napari, I.; Lehtinen, K. E. J.; Timmreck, C.; Noppel, M.; Laaksonen, A. An Improved Parameterization for Sulfuric Acid−water Nucleation Rates for Tropospheric and Stratospheric Conditions. *J. Geophys. Res.: Atmos.* **2002**, *107*, AAC3−1−AAC3−10.

(61) Tilmes, S.; Mills, M. J.; Zhu, Y.; Bardeen, C. G.; Vitt, F.; Yu, P.; Fillmore, D.; Liu, X.; Toon, B.; Deshler, T. Description and Performance of the CARMA Sectional Aerosol Microphysical Model in CESM2. *Geosci. Model Dev. Discuss.* **2023**, 1−58.

(62) Jo, D. S.; Hodzic, A.; Emmons, L. K.; Tilmes, S.; Schwantes, R. H.; Mills, M. J.; Campuzano-Jost, P.; Hu, W.; Zaveri, R. A.; Easter, R. C.; Singh, B.; Lu, Z.; Schulz, C.; Schneider, J.; Shilling, J. E.; Wisthaler, A.; Jimenez, J. L. Future Changes in Isoprene-Epoxydiol-Derived Secondary Organic Aerosol (IEPOX SOA) under the Shared Socioeconomic Pathways: The Importance of Physicochemical Dependency. *Atmos. Chem. Phys.* **2021**, *21*, 3395−3425.

(63) Park, R. J.; Jacob, D. J.; Field, B. D.; Yantosca, R. M.; Chin, M. Natural and transboundary pollution influences on sulfate-nitrate-ammonium aerosols in the United States: Implications for policy. *J. Geophys. Res.: Atmos.* **2004**, *109* (), DOI: 10.1029/2003JD00473.

(64) Fountoukis, C.; Nenes, A. ISORROPIA II: A Computationally Effcient Thermodynamic Equilibrium Model for K^+−Ca^{2+}−Mg^{2+}−NH_4^+−Na^+−SO_4^{2-}−NO_3^-−Cl^-−H_2O Aerosols. *Atmos. Chem. Phys.* **2007**, *7*, 4639−4659.

(65) Gelaro, R.; McCarty, W.; Suárez, M. J.; Todling, R.; Molod, A.; Takacs, L.; Randles, C.; Darmenov, A.; Bosilovich, M. G.; Reichle, R.; Wargan, K.; Coy, L.; Cullather, R.; Draper, C.; Akella, S.; Buchard, V.; Conaty, A.; da Silva, A.; Gu, W.; Kim, G.-K.; Koster, R.; Lucchesi, R.; Merkova, D.; Nielsen, J. E.; Partyka, G.; Pawson, S.; Putman, W.; Rienecker, M.; Schubert, S. D.; Sienkiewicz, M.; Zhao, B. The Modern-Era Retrospective Analysis for Research and Applications, Version 2 (MERRA-2). *J. Clim.* **2017**, *30*, 5419−5454.

(66) Hoesly, R. M.; Smith, S. J.; Feng, L.; Klimont, Z.; Janssens-Maenhout, G.; Pitkanen, T.; Seibert, J. J.; Vu, L.; Andres, R. J.; Bolt, R. M.; Bond, T. C.; Dawidowski, L.; Kholod, N.; Kurokawa, J.-I.; Li, M.; Liu, L.; Lu, Z.; Moura, M. C. P.; O'Rourke, P. R.; Zhang, Q. Historical (1750−2014) Anthropogenic Emissions of Reactive Gases and Aerosols from the Community Emissions Data System (CEDS). *Geosci. Model Dev.* **2018**, *11*, 369−408.

(67) Giglio, L.; Randerson, J. T.; van der Werf, G. R. Analysis of daily, monthly, and annual burned area using the fourth-generation global fire emissions database (GFED4). *J. Geophys. Res.* **2013**, *118*, 317−328.

(68) Janssens-Maenhout, G.; Crippa, M.; Guizzardi, D.; Dentener, F.; Muntean, M.; Pouliot, G.; Keating, T.; Zhang, Q.; Kurokawa, J.; Wankmüller, R.; Others. HTAP_v2.2: a mosaic of regional and global emission grid maps for 2008 and 2010 to study hemispheric transport of air pollution. *Atmos. Chem. Phys.* **2015**, *15*, 11411−11432.

(69) Guenther, A. B.; Jiang, X.; Heald, C. L.; Sakulyanontvittaya, T.; Duhl, T.; Emmons, L. K.; Wang, X. The Model of Emissions of Gases and Aerosols from Nature Version 2.1 (MEGAN2.1): An Extended and Updated Framework for Modeling Biogenic Emissions. *Geosci. Model Dev.* **2012**, *5*, 1471−1492.

(70) Center for International Earth Science Information Network - CIESIN - Columbia University. Gridded Population of the World, Version 4 (GPWv4): Population Count, Revision 11. *NASA Socioeconomic Data Appl. Center (SEDAC)* **2018**, DOI: 10.7927/H4JW8BX5.

(71) Institute for Health Metrics and Evaluation (IHME). Global Burden of Disease Collaborative Network. Global Burden of Disease Study 2015 (GBD 2015) Life Expectancy, All-Cause and Cause-Specific Mortality 1980−2015. https://ghdx.healthdata.org/record/ihme-data/gbd-2015-life-expectancy-all-cause-and-cause-specific-mortality-1980-2015 (accessed 2023-03-25).

(72) Burnett, R. T.; Pope, C. A., III; Ezzati, M.; Olives, C.; Lim, S. S.; Mehta, S.; Shin, H. H.; Singh, G.; Hubbell, B.; Brauer, M.; Anderson, H. R.; Smith, K. R.; Balmes, J. R.; Bruce, N. G.; Kan, H.; Laden, F.; Prüss-Ustün, A.; Turner, M. C.; Gapstur, S. M.; Diver, W. R.; Cohen, A. An Integrated Risk Function for Estimating the Global Burden of Disease Attributable to Ambient Fine Particulate Matter Exposure. *Environ. Health Perspect.* **2014**, *122*, 397−403.
(73) Burnett, R. T.; Chen, H.; Szyszkowicz, M.; Fann, N.; Hubbell, B.; Pope, C. A., 3rd; Apte, J. S.; Brauer, M.; Cohen, A.; Weichenthal, S.; Coggins, J.; Di, Q.; Brunekreef, B.; Frostad, J.; Lim, S. S.; Kan, H.; Walker, K. D.; Thurston, G. D.; Hayes, R. B.; Lim, C. C.; Turner, M. C.; Jerrett, M.; Krewski, D.; Gapstur, S. M.; Diver, W. R.; Ostro, B.; Goldberg, D.; Crouse, D. L.; Martin, R. V.; Peters, P.; Pinault, L.; Tjepkema, M.; van Donkelaar, A.; Villeneuve, P. J.; Miller, A. B.; Yin, P.; Zhou, M.; Wang, L.; Janssen, N. A. H.; Marra, M.; Atkinson, R. W.; Tsang, H.; Quoc Thach, T.; Cannon, J. B.; Allen, R. T.; Hart, J. E.; Laden, F.; Cesaroni, G.; Forastiere, F.; Weinmayr, G.; Jaensch, A.; Nagel, G.; Concin, H.; Spadaro, J. V. Global estimates of mortality associated with long-term exposure to outdoor fine particulate matter. *Proc. Natl. Acad. Sci. U. S. A.* **2018**, *115*, 9592−9597.
(74) van Donkelaar, A.; Hammer, M. S.; Bindle, L.; Brauer, M.; Brook, J. R.; Garay, M. J.; Hsu, N. C.; Kalashnikova, O. V.; Kahn, R. A.; Lee, C.; Levy, R. C.; Lyapustin, A.; Sayer, A. M.; Martin, R. V. Monthly Global Estimates of Fine Particulate Matter and Their Uncertainty. *Environ. Sci. Technol.* **2021**, *55*, 15287−15300.
(75) van Donkelaar, A.; Martin, R. V.; Brauer, M.; Hsu, N. C.; Kahn, R. A.; Levy, R. C.; Lyapustin, A.; Sayer, A. M.; Winker, D. M. Global Estimates of Fine Particulate Matter Using a Combined Geophysical-Statistical Method with Information from Satellites, Models, and Monitors. *Environ. Sci. Technol.* **2016**, *50*, 3762−3772.
(76) Nawaz, M. O.; Henze, D. K.; Harkins, C.; Cao, H.; Nault, B.; Jo, D.; Jimenez, J.; Anenberg, S. C.; Goldberg, D. L.; Qu, Z. Impacts of Sectoral, Regional, Species, and Day-Specific Emissions on Air Pollution and Public Health in Washington, DC. *Elementa: Science of the Anthropocene* **2021**, *9*, No. 00043.
(77) Iacono, M. J.; Delamere, J. S.; Mlawer, E. J.; Shephard, M. W.; Clough, S. A.; Collins, W. D. Radiative Forcing by Long-Lived Greenhouse Gases: Calculations with the AER Radiative Transfer Models. *J. Geophys. Res.* **2008**, *113*, 233.
(78) Hess, M.; Koepke, P.; Schult, I. Optical Properties of Aerosols and Clouds: The Software Package OPAC. *Bull. Am. Meteorol. Soc.* **1998**, *79*, 831−844.
(79) Jimenez, J. L.; Canagaratna, M. R.; Donahue, N. M.; Prevot, A. S. H.; Zhang, Q.; Kroll, J. H.; DeCarlo, P. F.; Allan, J. D.; Coe, H.; Ng, N. L.; Aiken, A. C.; Docherty, K. S.; Ulbrich, I. M.; Grieshop, A. P.; Robinson, A. L.; Duplissy, J.; Smith, J. D.; Wilson, K. R.; Lanz, V. A.; Hueglin, C.; Sun, Y. L.; Tian, J.; Laaksonen, A.; Raatikainen, T.; Rautiainen, J.; Vaattovaara, P.; Ehn, M.; Kulmala, M.; Tomlinson, J. M.; Collins, D. R.; Cubison, M. J.; Dunlea, E. J.; Huffman, J. A.; Onasch, T. B.; Alfarra, M. R.; Williams, P. I.; Bower, K.; Kondo, Y.; Schneider, J.; Drewnick, F.; Borrmann, S.; Weimer, S.; Demerjian, K.; Salcedo, D.; Cottrell, L.; Griffin, R.; Takami, A.; Miyoshi, T.; Hatakeyama, S.; Shimono, A.; Sun, J. Y.; Zhang, Y. M.; Dzepina, K.; Kimmel, J. R.; Sueper, D.; Jayne, J. T.; Herndon, S. C.; Trimborn, A. M.; Williams, L. R.; Wood, E. C.; Middlebrook, A. M.; Kolb, C. E.; Baltensperger, U.; Worsnop, D. R. Evolution of organic aerosols in the atmosphere. *Science* **2009**, *326*, 1525−1529.
(80) Drury, E.; Jacob, D. J.; Spurr, R. J. D.; Wang, J.; Shinozuka, Y.; Anderson, B. E.; Clarke, A. D.; Dibb, J.; McNaughton, C.; Weber, R. Synthesis of Satellite (MODIS), Aircraft (ICARTT), and Surface (IMPROVE, EPA-AQS, AERONET) Aerosol Observations over Eastern North America to Improve MODIS Aerosol Retrievals and Constrain Surface Aerosol Concentrations and Sources. *J. Geophys. Res.* **2010**, *115*, 204.
(81) Latimer, R. N. C.; Martin, R. V. Interpretation of Measured Aerosol Mass Scattering Efficiency over North America Using a Chemical Transport Model. *Atmos. Chem. Phys.* **2019**, *19*, 2635−2653.
(82) Mills, M. J.; Schmidt, A.; Easter, R.; Solomon, S.; Kinnison, D. E.; Ghan, S. J.; Neely, R. R., III; Marsh, D. R.; Conley, A.; Bardeen, C. G.; Gettelman, A. Global Volcanic Aerosol Properties Derived from Emissions, 1990−2014, Using CESM1(WACCM). *J. Geophys. Res.* **2016**, *121*, 2332−2348.
(83) Morrison, H.; Gettelman, A. A New Two-Moment Bulk Stratiform Cloud Microphysics Scheme in the Community Atmosphere Model, Version 3 (CAM3). Part I: Description and Numerical Tests. *J. Clim.* **2008**, *21*, 3642−3659.
(84) Twomey, S. The Influence of Pollution on the Shortwave Albedo of Clouds. *J. Atmos. Sci.* **1977**, *34*, 1149−1152.
(85) Albrecht, B. A. Aerosols, Cloud Microphysics, and Fractional Cloudiness. *Science* **1989**, *245*, 1227−1230.
(86) Gettelman, A.; Sherwood, S. C. Processes Responsible for Cloud Feedback. *Curr. Clim. Change Rep.* **2016**, *2*, 179−189.
(87) Park, R. J.; Jacob, D. J.; Kumar, N.; Yantosca, R. M. Regional visibility statistics in the United States: Natural and transboundary pollution influences, and implications for the Regional Haze Rule. *Atmos. Environ.* **2006**, *40*, 5405−5423.
(88) Heald, C. L.; Collett, J. L., Jr.; Lee, T.; Benedict, K. B.; Schwandner, F. M.; Li, Y.; Clarisse, L.; Hurtmans, D. R.; Van Damme, M.; Clerbaux, C.; Coheur, P.-F.; Philip, S.; Martin, R. V.; Pye, H. O. T. Atmospheric ammonia and particulate inorganic nitrogen over the United States. *Atmos. Chem. Phys.* **2012**, *12*, 10295−10312.
(89) Walker, J. M.; Philip, S.; Martin, R. V.; Seinfeld, J. H. Simulation of Nitrate, Sulfate, and Ammonium Aerosols over the United States. *Atmos. Chem. Phys.* **2012**, *12*, 11213−11227.
(90) Jeong, J. I.; Park, R. J. Winter Monsoon Variability and Its Impact on Aerosol Concentrations in East Asia. *Environ. Pollut.* **2017**, *221*, 285−292.
(91) Fairlie, T. D.; Liu, H.; Vernier, J.; Campuzano-Jost, P.; Jimenez, J. L.; Jo, D. S.; Zhang, B.; Natarajan, M.; Avery, M. A.; Huey, G. Estimates of Regional Source Contributions to the Asian Tropopause Aerosol Layer Using a Chemical Transport Model. *J. Geophys. Res.: Atmos.* **2020**, *125*, No. e2019JD031506.
(92) Jeong, J. I.; Jo, D. S.; Park, R. J.; Lee, H.-M.; Curci, G.; Kim, S.-W. Parametric Analysis for Global Single Scattering Albedo Calculations. *Atmos. Environ.* **2020**, *234*, No. 117616.
(93) Park, R. J.; Oak, Y. J.; Emmons, L. K.; Kim, C.-H.; Pfister, G. G.; Carmichael, G. R.; Saide, P. E.; Cho, S.-Y.; Kim, S.; Woo, J.-H.; Crawford, J. H.; Gaubert, B.; Lee, H.-J.; Park, S.-Y.; Jo, Y.-J.; Gao, M.; Tang, B.; Stanier, C. O.; Shin, S. S.; Park, H. Y.; Bae, C.; Kim, E. Multi-Model Intercomparisons of Air Quality Simulations for the KORUS-AQ Campaign. *Elementa: Science of the Anthropocene* **2021**, *9* (), DOI: 10.1525/elementa.2021.00139.
(94) Fung, K. M.; Heald, C. L.; Kroll, J. H.; Wang, S.; Jo, D. S.; Gettelman, A.; Lu, Z.; Liu, X.; Zaveri, R. A.; Apel, E. C.; Blake, D. R.; Jimenez, J.-L.; Campuzano-Jost, P.; Veres, P. R.; Bates, T. S.; Shilling, J. E.; Zawadowicz, M. Exploring Dimethyl Sulfide (DMS) Oxidation and Implications for Global Aerosol Radiative Forcing. *Atmos. Chem. Phys.* **2022**, *22*, 1549−1573.
(95) Travis, K. R.; Crawford, J. H.; Chen, G.; Jordan, C. E.; Nault, B. A.; Kim, H.; Jimenez, J. L.; Campuzano-Jost, P.; Dibb, J. E.; Woo, J.-H.; Kim, Y.; Zhai, S.; Wang, X.; McDuffie, E. E.; Luo, G.; Yu, F.; Kim, S.; Simpson, I. J.; Blake, D. R.; Chang, L.; Kim, M. J. Limitations in Representation of Physical Processes Prevent Successful Simulation of $PM_{2.5}$ during KORUS-AQ. *Atmos. Chem. Phys.* **2022**, *22*, 7933−7958.
(96) Nault, B. A.; Campuzano-Jost, P.; Day, D. A.; Jo, D. S.; Schroder, J. C.; Allen, H. M.; Bahreini, R.; Bian, H.; Blake, D. R.; Chin, M.; Clegg, S. L.; Colarco, P. R.; Crounse, J. D.; Cubison, M. J.; DeCarlo, P. F.; Dibb, J. E.; Diskin, G. S.; Hodzic, A.; Hu, W.; Katich, J. M.; Kim, M. J.; Kodros, J. K.; Kupc, A.; Lopez-Hilfiker, F. D.; Marais, E. A.; Middlebrook, A. M.; Andrew Neuman, J.; Nowak, J. B.; Palm, B. B.; Paulot, F.; Pierce, J. R.; Schill, G. P.; Scheuer, E.; Thornton, J. A.; Tsigaridis, K.; Wennberg, P. O.; Williamson, C. J.; Jimenez, J. L. Chemical Transport Models Often Underestimate Inorganic Aerosol Acidity in Remote Regions of the Atmosphere. *Commun. Earth Environ.* **2021**, *2*, 1−13.

(97) Lelieveld, J.; Evans, J. S.; Fnais, M.; Giannadaki, D.; Pozzer, A. The contribution of outdoor air pollution sources to premature mortality on a global scale. *Nature* **2015**, *525*, 367−371.
(98) Lim, S. S.; Vos, T.; Flaxman, A. D.; Danaei, G.; Shibuya, K.; Adair-Rohani, H.; Amann, M.; Anderson, H. R.; Andrews, K. G.; Aryee, M.; Atkinson, C.; Bacchus, L. J.; Bahalim, A. N.; Balakrishnan, K.; Balmes, J.; Barker-Collo, S.; Baxter, A.; Bell, M. L.; Blore, J. D.; Blyth, F.; Bonner, C.; Borges, G.; Bourne, R.; Boussinesq, M.; Brauer, M.; Brooks, P.; Bruce, N. G.; Brunekreef, B.; Bryan-Hancock, C.; Bucello, C.; Buchbinder, R.; Bull, F.; Burnett, R. T.; Byers, T. E.; Calabria, B.; Carapetis, J.; Carnahan, E.; Chafe, Z.; Charlson, F.; Chen, H.; Chen, J. S.; Cheng, A. T.-A.; Child, J. C.; Cohen, A.; Colson, K. E.; Cowie, B. C.; Darby, S.; Darling, S.; Davis, A.; Degenhardt, L.; Dentener, F.; Des Jarlais, D. C.; Devries, K.; Dherani, M.; Ding, E. L.; Dorsey, E. R.; Driscoll, T.; Edmond, K.; Ali, S. E.; Engell, R. E.; Erwin, P. J.; Fahimi, S.; Falder, G.; Farzadfar, F.; Ferrari, A.; Finucane, M. M.; Flaxman, S.; Fowkes, F. G. R.; Freedman, G.; Freeman, M. K.; Gakidou, E.; Ghosh, S.; Giovannucci, E.; Gmel, G.; Graham, K.; Grainger, R.; Grant, B.; Gunnell, D.; Gutierrez, H. R.; Hall, W.; Hoek, H. W.; Hogan, A.; Hosgood, H. D., 3rd; Hoy, D.; Hu, H.; Hubbell, B. J.; Hutchings, S. J.; Ibeanusi, S. E.; Jacklyn, G. L.; Jasrasaria, R.; Jonas, J. B.; Kan, H.; Kanis, J. A.; Kassebaum, N.; Kawakami, N.; Khang, Y.-H.; Khatibzadeh, S.; Khoo, J.-P.; Kok, C.; Laden, F.; Lalloo, R.; Lan, Q.; Lathlean, T.; Leasher, J. L.; Leigh, J.; Li, Y.; Lin, J. K.; Lipshultz, S. E.; London, S.; Lozano, R.; Lu, Y.; Mak, J.; Malekzadeh, R.; Mallinger, L.; Marcenes, W.; March, L.; Marks, R.; Martin, R.; McGale, P.; McGrath, J.; Mehta, S.; Mensah, G. A.; Merriman, T. R.; Micha, R.; Michaud, C.; Mishra, V.; Mohd Hanafiah, K.; Mokdad, A. A.; Morawska, L.; Mozaffarian, D.; Murphy, T.; Naghavi, M.; Neal, B.; Nelson, P. K.; Nolla, J. M.; Norman, R.; Olives, C.; Omer, S. B.; Orchard, J.; Osborne, R.; Ostro, B.; Page, A.; Pandey, K. D.; Parry, C. D. H.; Passmore, E.; Patra, J.; Pearce, N.; Pelizzari, P. M.; Petzold, M.; Phillips, M. R.; Pope, D.; Pope, C. A., 3rd; Powles, J.; Rao, M.; Razavi, H.; Rehfuess, E. A.; Rehm, J. T.; Ritz, B.; Rivara, F. P.; Roberts, T.; Robinson, C.; Rodriguez-Portales, J. A.; Romieu, I.; Room, R.; Rosenfeld, L. C.; Roy, A.; Rushton, L.; Salomon, J. A.; Sampson, U.; Sanchez-Riera, L.; Sanman, E.; Sapkota, A.; Seedat, S.; Shi, P.; Shield, K.; Shivakoti, R.; Singh, G. M.; Sleet, D. A.; Smith, E.; Smith, K. R.; Stapelberg, N. J. C.; Steenland, K.; Stöckl, H.; Stovner, L. J.; Straif, K.; Straney, L.; Thurston, G. D.; Tran, J. H.; Van Dingenen, R.; van Donkelaar, A.; Veerman, J. L.; Vijayakumar, L.; Weintraub, R.; Weissman, M. M.; White, R. A.; Whiteford, H.; Wiersma, S. T.; Wilkinson, J. D.; Williams, H. C.; Williams, W.; Wilson, N.; Woolf, A. D.; Yip, P.; Zielinski, J. M.; Lopez, A. D.; Murray, C. J. L.; Ezzati, M.; AlMazroa, M. A.; Memish, Z. A. A Comparative Risk Assessment of Burden of Disease and Injury Attributable to 67 Risk Factors and Risk Factor Clusters in 21 Regions, 1990-2010: A Systematic Analysis for the Global Burden of Disease Study 2010. *Lancet* **2012**, *380*, 2224−2260.
(99) Lelieveld, J.; Klingmüller, K.; Pozzer, A.; Burnett, R. T.; Haines, A.; Ramanathan, V. Effects of fossil fuel and total anthropogenic emission removal on public health and climate. *Proc. Natl. Acad. Sci. U. S. A.* **2019**, *116*, 7192−7197.
(100) Rémy, S.; Veira, A.; Paugam, R.; Sofiev, M.; Kaiser, J. W.; Marenco, F.; Burton, S. P.; Benedetti, A.; Engelen, R. J.; Ferrare, R.; Hair, J. W. Two Global Data Sets of Daily Fire Emission Injection Heights since 2003. *Atmos. Chem. Phys.* **2017**, *17*, 2921−2942.
(101) Palmer, P. I.; Marvin, M. R.; Siddans, R.; Kerridge, B. J.; Moore, D. P. Nocturnal Survival of Isoprene Linked to Formation of Upper Tropospheric Organic Aerosol. *Science* **2022**, *375*, 562−566.
(102) Loeb, N. G.; Doelling, D. R.; Wang, H.; Su, W.; Nguyen, C.; Corbett, J. G.; Liang, L.; Mitrescu, C.; Rose, F. G.; Kato, S. Clouds and the Earth's Radiant Energy System (CERES) Energy Balanced and Filled (EBAF) Top-of-Atmosphere (TOA) Edition-4.0 Data Product. *J. Clim.* **2018**, *31*, 895−918.
(103) Yang, Y.; Wang, H.; Smith, S. J.; Easter, R.; Ma, P.-L.; Qian, Y.; Yu, H.; Li, C.; Rasch, P. J. Global Source Attribution of Sulfate Concentration and Direct and Indirect Radiative Forcing. *Atmos. Chem. Phys.* **2017**, *17*, 8903−8922.
(104) Shrivastava, M.; Easter, R. C.; Liu, X.; Zelenyuk, A.; Singh, B.; Zhang, K.; Ma, P.-L.; Chand, D.; Ghan, S.; Jimenez, J. L.; Zhang, Q.; Fast, J.; Rasch, P. J.; Tiitta, P. Global Transformation and Fate of SOA: Implications of Low-Volatility SOA and Gas-Phase Fragmentation Reactions. *J. Geophys. Res.* **2015**, *120*, 4169−4195.
(105) Jo, D. S.; Park, R. J.; Lee, S.; Kim, S.-W.; Zhang, X. A global simulation of brown carbon: implications for photochemistry and direct radiative effect. *Atmos. Chem. Phys.* **2016**, *16*, 3413−3432.
(106) Henze, D. K.; Shindell, D. T.; Akhtar, F.; Spurr, R. J. D.; Pinder, R. W.; Loughlin, D.; Kopacz, M.; Singh, K.; Shim, C. Spatially Refined Aerosol Direct Radiative Forcing Efficiencies. *Environ. Sci. Technol.* **2012**, *46*, 9511−9518.
(107) Haywood, J.; Boucher, O. Estimates of the direct and indirect radiative forcing due to tropospheric aerosols: A review. *Rev. Geophys.* **2000**, *38*, 513−543.
(108) Yu, H.; Dickinson, R. E.; Chin, M.; Kaufman, Y. J.; Zhou, M.; Zhou, L.; Tian, Y.; Dubovik, O.; Holben, B. N. Direct Radiative Effect of Aerosols as Determined from a Combination of MODIS Retrievals and GOCART Simulations. *J. Geophys. Res.* **2004**, *109* (), DOI: 10.1029/2003jd003914.
(109) Thornhill, G. D.; Collins, W. J.; Kramer, R. J.; Olivié, D.; Skeie, R. B.; O'Connor, F. M.; Abraham, N. L.; Checa-Garcia, R.; Bauer, S. E.; Deushi, M.; Emmons, L. K.; Forster, P. M.; Horowitz, L. W.; Johnson, B.; Keeble, J.; Lamarque, J.-F.; Michou, M.; Mills, M. J.; Mulcahy, J. P.; Myhre, G.; Nabat, P.; Naik, V.; Oshima, N.; Schulz, M.; Smith, C. J.; Takemura, T.; Tilmes, S.; Wu, T.; Zeng, G.; Zhang, J. Effective Radiative Forcing from Emissions of Reactive Gases and Aerosols − a Multi-Model Comparison. *Atmos. Chem. Phys.* **2021**, *21*, 853−874.
(110) Koren, I.; Dagan, G.; Altaratz, O. From Aerosol-Limited to Invigoration of Warm Convective Clouds. *Science* **2014**, *344*, 1143−1146.
(111) Gettelman, A.; Bardeen, C. G.; McCluskey, C. S.; Järvinen, E.; Stith, J.; Bretherton, C.; McFarquhar, G.; Twohy, C.; D'Alessandro, J.; Wu, W. Simulating Observations of Southern Ocean Clouds and Implications for Climate. *J. Geophys. Res.* **2020**, *125* (), DOI: 10.1029/2020jd032619.
(112) Koren, I.; Martins, J. V.; Remer, L. A.; Afargan, H. Smoke Invigoration versus Inhibition of Clouds over the Amazon. *Science* **2008**, *321*, 946−949.
(113) Pye, H. O. T.; Ward-Caviness, C. K.; Murphy, B. N.; Appel, K. W.; Seltzer, K. M. Secondary Organic Aerosol Association with Cardiorespiratory Disease Mortality in the United States. *Nat. Commun.* **2021**, *12*, 7215.
(114) Soleimanian, E.; Mousavi, A.; Taghvaee, S.; Shafer, M. M.; Sioutas, C. Impact of Secondary and Primary Particulate Matter (PM) Sources on the Enhanced Light Absorption by Brown Carbon (BrC) Particles in Central Los Angeles. *Sci. Total Environ.* **2020**, *705*, No. 135902.
(115) Xiong, R.; Li, J.; Zhang, Y.; Zhang, L.; Jiang, K.; Zheng, H.; Kong, S.; Shen, H.; Cheng, H.; Shen, G.; Tao, S. Global Brown Carbon Emissions from Combustion Sources. *Environ. Sci. Ecotechnol.* **2022**, *12*, No. 100201.
(116) Zeng, L.; Dibb, J.; Scheuer, E.; Katich, J. M.; Schwarz, J. P.; Bourgeois, I.; Peischl, J.; Ryerson, T.; Warneke, C.; Perring, A. E.; Diskin, G. S.; DiGangi, J. P.; Nowak, J. B.; Moore, R. H.; Wiggins, E. B.; Pagonis, D.; Guo, H.; Campuzano-Jost, P.; Jimenez, J. L.; Xu, L.; Weber, R. J. Characteristics and Evolution of Brown Carbon in Western United States Wildfires. *Atmos. Chem. Phys.* **2022**, *22*, 8009−8036.
(117) Feng, Y.; Ramanathan, V.; Kotamarthi, V. R. Brown carbon: a significant atmospheric absorber of solar radiation? *Atmos. Chem. Phys.* **2013**, *13*, 8607−8621.
(118) Brown, H.; Liu, X.; Feng, Y.; Jiang, Y.; Wu, M.; Lu, Z.; Wu, C.; Murphy, S.; Pokhrel, R. Radiative Effect and Climate Impacts of Brown Carbon with the Community Atmosphere Model (CAM5). *Atmos. Chem. Phys.* **2018**, *18*, 17745−17768.

(119) Yan, J.; Wang, X.; Gong, P.; Wang, C.; Cong, Z. Review of Brown Carbon Aerosols: Recent Progress and Perspectives. *Sci. Total Environ.* **2018**, *634*, 1475−1485.
(120) Wang, X.; Heald, C. L.; Liu, J.; Weber, R. J.; Campuzano-Jost, P.; Jimenez, J. L.; Schwarz, J. P.; Perring, A. E. Exploring the Observational Constraints on the Simulation of Brown Carbon. *Atmos. Chem. Phys.* **2018**, *18*, 635−653.
(121) Seinfeld, J. H.; Bretherton, C.; Carslaw, K. S.; Coe, H.; DeMott, P. J.; Dunlea, E. J.; Feingold, G.; Ghan, S.; Guenther, A. B.; Kahn, R.; Kraucunas, I.; Kreidenweis, S. M.; Molina, M. J.; Nenes, A.; Penner, J. E.; Prather, K. A.; Ramanathan, V.; Ramaswamy, V.; Rasch, P. J.; Ravishankara, A. R.; Rosenfeld, D.; Stephens, G.; Wood, R. Improving Our Fundamental Understanding of the Role of Aerosol−cloud Interactions in the Climate System. *Proc. Natl. Acad. Sci.* **2016**, *113*, 5781−5790.
(122) Gettelman, A.; Hannay, C.; Bacmeister, J. T.; Neale, R. B.; Pendergrass, A. G.; Danabasoglu, G.; Lamarque, J. F.; Fasullo, J. T.; Bailey, D. A.; Lawrence, D. M.; Mills, M. J. High Climate Sensitivity in the Community Earth System Model Version 2 (CESM2). *Geophys. Res. Lett.* **2019**, *46*, 8329−8337.
(123) Hasekamp, O. P.; Gryspeerdt, E.; Quaas, J. Analysis of Polarimetric Satellite Measurements Suggests Stronger Cooling due to Aerosol-Cloud Interactions. *Nat. Commun.* **2019**, *10*, 5405.
(124) Edwards, D. P.; Emmons, L. K.; Gille, J. C.; Chu, A.; Attié, J.-L.; Giglio, L.; Wood, S. W.; Haywood, J.; Deeter, M. N.; Massie, S. T.; Ziskin, D. C.; Drummond, J. R. Satellite-Observed Pollution from Southern Hemisphere Biomass Burning. *J. Geophys. Res.* **2006**, *111* (), DOI: 10.1029/2005jd006655.
(125) Schill, G. P.; Froyd, K. D.; Bian, H.; Kupc, A.; Williamson, C.; Brock, C. A.; Ray, E.; Hornbrook, R. S.; Hills, A. J.; Apel, E. C.; Chin, M.; Colarco, P. R.; Murphy, D. M. Widespread Biomass Burning Smoke throughout the Remote Troposphere. *Nat. Geosci.* **2020**, *13*, 422−427.
(126) Williamson, C. J.; Kupc, A.; Axisa, D.; Bilsback, K. R.; Bui, T.; Campuzano-Jost, P.; Dollner, M.; Froyd, K. D.; Hodshire, A. L.; Jimenez, J. L.; Kodros, J. K.; Luo, G.; Murphy, D. M.; Nault, B. A.; Ray, E. A.; Weinzierl, B.; Wilson, J. C.; Yu, F.; Yu, P.; Pierce, J. R.; Brock, C. A. A Large Source of Cloud Condensation Nuclei from New Particle Formation in the Tropics. *Nature* **2019**, *574*, 399−403.
(127) Kupc, A.; Williamson, C. J.; Hodshire, A. L.; Kazil, J.; Ray, E.; Bui, T. P.; Dollner, M.; Froyd, K. D.; McKain, K.; Rollins, A.; Schill, G. P.; Thames, A.; Weinzierl, B. B.; Pierce, J. R.; Brock, C. A. The Potential Role of Organics in New Particle Formation and Initial Growth in the Remote Tropical Upper Troposphere. *Atmos. Chem. Phys.* **2020**, *20*, 15037−15060.
(128) Tsigaridis, K.; Kanakidou, M. The Present and Future of Secondary Organic Aerosol Direct Forcing on Climate. *Curr. Clim. Change Rep.* **2018**, *4*, 84−98.
(129) Jo, D. S.; Tilmes, S.; Emmons, L. K.; Wang, S.; Vitt, F. A New Simplified Parameterization of Secondary Organic Aerosol in the Community Earth System Model Version 2 (CESM2; CAM6.3). *Geosci. Model Dev.* **2023**, *16*, 3893−3906.

https://doi.org/10.1021/acs.est.3c02823
Environ. Sci. Technol. 2023, 57, 13793−13807